NTIA Report 89-249

# Millimeter-Wave Propagation in the Mesosphere

G. A. Hufford
H. J. Liebe

U.S. DEPARTMENT OF COMMERCE
Robert A. Mosbacher, Secretary

Janice Obuchowski, Assistant Secretary
for Communications and Information

September 1989

## PREFACE

Certain commercial equipment and software products are identified in this report to adequately describe the design and operation of the program reported here. In no case does such identification imply recommendation or endorsement by the National Telecommunications and Information Administration, nor does it imply that the material or equipment identified is necessarily the best available for the purpose.

## CONTENTS


| | | Page |
|---|---|---|
| 1. | INTRODUCTION | 1 |
| 2. | THE OXYGEN ABSORPTION LINES NEAR 60 GHz | 2 |
| 2.1 | Line Properties in the Absence of a Magnetic Field | 2 |
| 2.2 | The Geomagnetic Field and the Zeeman Effect | 8 |
| 3. | RADIO WAVE PROPAGATION IN THE ANISOTROPIC MESOSPHERE | 17 |
| 3.1 | Basic Equations for Plane-Wave Propagation | 17 |
| 3.2 | The Refractivity Matrix | 19 |
| 3.3 | Characteristic Waves | 22 |
| 3.4 | Polarization and Stokes Parameters | 25 |
| 3.5 | Symmetries and Other Properties of the Characteristic Waves | 28 |
| 4. | FEATURES OF THE PROGRAM "ZEEMAN" | 33 |
| 4.1 | N Components | 36 |
| 4.2 | Eigenvalues | 36 |
| 4.3 | Characteristic Waves | 36 |
| 4.4 | Radio Wave Propagation | 42 |
| 4.5 | Propagation Through the Mesosphere | 47 |
| 5. | CONCLUSIONS | 50 |
| 6. | ACKNOWLEDGMENT | 50 |
| 7. | REFERENCES | 50 |

## LIST OF FIGURES


Page

Figure 1. Normalized Voight profiles of absorption u and v. Shown are profiles versus frequency x at constant pressure y (solid curves) and the pressure profiles of maximum absorption $u_o$ and peak dispersion $v_o$. . . . . 7

Figure 2. Pressure-broadened oxygen microwave lines in dry air for conditions at about 30 km altitude with p = w kPa, T = 225 K; at top is the attenuation spectrum and at bottom is the delay spectrum. . . . . 9

Figure 3. Schematic energy level diagram displaying the Zeeman components for the $3^+$ and $3^-$ oxygen microwave lines. In actuality, the energy levels for J = K±1 both lie below that for J = K. . . . . 11

Figure 4. Schematic plots of the frequency shifts $\eta$ and relative intensity factors $\xi$ for the Zeeman components of the $1^\pm$ to $7^\pm$ oxygen lines. . . . . 14

Figure 5. Attenuation patterns of the $7^+$ oxygen line for altitudes from 30 to 100 km. Each frame displays the three separate patterns for magnetic flux densities of 30 and 60 $\mu$T. . . . . 15

Figure 6. Magnitude of the magnetic flux density as given by the International Geomagnetic Reference Field of 1985. . . . . 34

Figure 7. The first few screens displayed by program ZEEMAN. . . . . 35

Figure 8. The "Summary of Parameters" for the "Default Case" for program ZEEMAN. . . . . 37

Figure 9. Real and imaginary parts of the N components for the Default Case. . . . . 38

Figure 10. The tabular display of the N components for the Default Case. . . . . 39

Figure 11. The eigenvalues for the Default Case. Real parts and imaginary parts plotted against the angle $\phi$. . . . . 40

Figure 12. The eigenvalues for the Default Case. Real parts and imaginary parts plotted against the frequency deviation $\Delta f$ . . . . . 41

Figure 13. The eigenvalues for the Default Case where, however, $\Delta f = 0$. Real parts and imaginary parts plotted against the angle $\phi$. . . . . 43

## LIST OF FIGURES (CONT.)


Page

Figure 14. Normalized Stokes parameters of the eigenvectors for the Default Case plotted against the angle $\phi$. . . . . 44

Figure 15. Trajectories of the eigenvectors for the Default Case as plotted on the Poincaré sphere. . . . . 44

Figure 16. The trajectory on the Poincaré sphere of a wave propagating through mesospheric-like medium. Parameters are those of the Default Case. . . . . 45

Figure 17. Attenuation versus distances for the wave in Figure 16. . . . . 46

Figure 18. Elliptical trajectories of the electric field at selected distance for the wave depicted in Figure 16. . . . . 46

Figure 19. Total attenuation and elliptical trajectories of the electric field after a wave has emerged from the top of the mesosphere. Initial parameters are those of the Default Case and initial polarizations are left. . . . . 48

Figure 20. Tabular display showing how a radio wave progresses through the mesosphere. Input parameters are those of the Default Case. . . . . 48

Figure 21. Total attenuation versus frequency deviation for waves emerging from the top of the mesosphere. Initial conditions are those of the Default Case. Top: vertical polarization beginning above and crossing beneath horizontal polarization. Bottom: right circular polarization beginning above and crossing beneath left circular polarization. . . . . 49

## LIST OF TABLES


Page

Table 1. Line Frequencies and Coefficients for Microwave Trasnitions of $O_2$ in Air . . . . . 5

Table 2. Temperature and Pressure in the Mesosphere. (U.S. Standard Atmosphere, 1976) . . . . . 6

Table 3. Coefficients for the Zeeman Components . . . . . 12

Table 4. The Frequency Shifts $\eta$ and Relative Intensity Factors $\xi$ for the Zeeman Components of the 1± to 7± Oxygen Lines . . . . 13

# MILLIMETER-WAVE PROPAGATION IN THE MESOSPHERE

George A. Hufford and Hans J. Liebe*

At heights between 30 and 100 km above Earth, the oxygen absorption lines near 60 GHz together with the geomagnetic field cause the atmosphere to become an anisotropic medium. This report discusses why this is so and how to compute the consequent effects. It describes the computer program ZEEMAN, which allows the user to display in either graphical or tabular form many aspects of how radio waves propagate through this medium.

Key words: anisotropic media; mesosphere; millimeter waves; oxygen absorption lines; polarization; radio propagation; Zeeman effect

## 1. INTRODUCTION

The mesosphere is that portion of Earth's atmosphere that lies between the stratosphere and the thermosphere from somewhat above 30 km in altitude to less than 100 km. The air is tenuous, and pressures vary from 1 to $10^{-4}$ kPa. Nevertheless, the oxygen absorption lines near 60 GHz are still strong enough to affect radio propagation.

Because the pressure is low, the lines are very sharp and a new phenomenon appears. This is the Zeeman effect induced by the geomagnetic field. Each line splits into a number of sublines; and how these sublines react to an electromagnetic field depends on the polarization of that field. There is, therefore, a small portion of the spectrum where the medium is anisotropic so that radio waves propagating through it are subject to such consequences as polarization discrimination and Faraday rotation. The physical reasons for this behavior are discussed in Townes and Schawlow (1955, especially Chapter 11). Engineering characterizations are given in Gautier (1967), Lenoir (1968), Liebe (1981, 1983), Hartman and Künzi (1983), and Rosenkranz and Staelin (1988). This report will summarize these results and show how they may be used to describe radio wave propagation in this medium. The final sections describe a computer program ZEEMAN, which allows a user to choose a scenario involving radio propagation at a point above Earth and to compute properties of the resultant propagation effects.

---

*The authors are with the Institute for Telecommunication Sciences, National Telecommunications and Information Administration, U.S. Department of Commerce, Boulder, CO 80303.

## 2. THE OXYGEN ABSORPTION LINES NEAR 60 GHz

In this section, we define a model describing the electromagnetic properties of the mesospheric atmosphere. We begin with the case when there is no geomagnetic field, and we shall describe the nearly 40 oxygen obsorption lines that lie near 60 GHz. Later, we shall consider the effect of a static magnetic field on a single one of these lines.

### 2.1 Line Properties in the Absence of a Magnetic Field

Gaseous molecules tumble about in space and vibrate internally, and the motion requires energy that is confined to a set of discrete quantum levels. A transition between two of these levels is accompanied by the absorption or emission of electromagnetic energy at a precise frequency, thus marking out a spectral line.

Most molecules that have absorption lines at radio frequencies interact with the electromagnetic field because they have an electric dipole moment. The $O_2$ molecule, however, is quite symmetrical with its 16 electrons evenly distributed. It has no electric dipole moment and therefore cannot interact with the electric field. On the other hand, the molecule in its normal state does have one rather subtle asymmetry--nine of its electrons spin in one direction while seven spin in the other. The resultant total spin provides a *magnetic* dipole moment. The oxygen molecule is paramagnetic and interacts with the magnetic component of the electromagnetic field.

Rotational energy levels of a linear gaseous molecule (having one principle moment of inertia) arise from the angular momentum associated with its tumbling action. Approximate values are given by the formula $BK(K+1)$, where B is related to the moment of inertia of the molecule and the "quantum number" K may be any nonnegative integer. In particular, this is true of the $O_2$ molecule except that symmetry again intervenes, and because of the Pauli exclusion principle, it turns out that only odd K are allowed. This produces the "orbital angular momentum" levels.

The 60-GHz lines do not come directly from those levels but from their "fine structure." The electron spin again enters the picture and now becomes an additional independent component of the angular momentum. Since electrons have spin 1/2, the total electron spin of the normal oxygen molecule is 1, and this adds vectorially into the resultant angular momentum. It follows that

for each K, the "total angular momentum" takes on values J=K-1, K, and K+1, so that each energy level has split into three.

When these three fine structure levels interact with an electromagnetic field, there are "selection rules" which in this case say that transitions can take place only between adjacent quantum numbers. Thus there can be transitions between the K and K+1 levels and between the K and K-1 levels. These produce what are called the $K^+$ and $K^-$ absorption lines, respectively.

To the engineer, these absorption lines show themselves as resonances in the complex refractivity of the atmosphere. Following Liebe (1983), we write

$$N = N_s + N'(f) + iN''(f) \tag{1}$$

where $N_s$ is a frequency-independent refractivity, $N'$ is a refractive dispersion, and $N''$ is the absorption term. These are all small numbers and normally they are measured in parts per million (sometimes called N-units). Free propagation of a plane wave in the z-direction is then given by

$$E(z) = \exp[ikz(1 + N)]\, E_o \tag{2}$$

where $E(z)$ is the electric field at $z$, $E_o$ is the initial electric field at $z = 0$, and $k = 2\pi f/c$ is the free space wave number. In more practical terminology, we have the specific attenuation $\alpha$, the excess phase lag $\beta$, and the specific delay time $\tau$ given by

$$\begin{aligned} \alpha &= 0.1820\ f\ N''(f) && \text{dB/km}, \\ \beta &= 1.2008\ f\ [N_s + N'(f)] && \text{deg/km}, \\ \tau &= 3.3356\ [N_s + N'(f)] && \text{ps/km}, \end{aligned} \tag{3}$$

where f is to be measured in gigahertz and the refractivities in parts per million.

In this report, we shall restrict ourselves to frequencies near 60 GHz and to conditions that resemble the atmosphere above 30 km altitude where the air is dry and the environmental parameters of concern are pressure P and temperature T. We suppose P is measured in kilopascal, and define a "relative inverse temperature," $\theta = 300/T$, where T is the absolute temperature in kelvin. Then our model for the refractivity sets

$$N_s = 2.5892\ P\theta \qquad \text{ppm} \tag{4}$$

and

$$N' + iN'' = \sum_n (SF)_n \qquad \text{ppm}\ , \tag{5}$$

where S is a line strength and F a Lorentzian line shape function

$$F(f) = 1/(\nu_o - f - i\gamma) \tag{6}$$

with the line center frequency $\nu_o$ and the line width $\gamma$. One measures S in kilohertz and the frequencies in the denominator of F in gighertz, thus building in a factor of $10^6$ to produce the refractivity units.

The center frequencies have fixed values but the strengths and widths are to be calculated from

$$S = a_1 P\theta^3 \exp[a_2(1 - \theta)] \qquad \text{kHz} \tag{7}$$

and

$$\gamma = a_3 P\theta^{0.8} \qquad \text{GHz} \tag{8}$$

The line center frequencies $\nu_o$ (Endo and Mizushima, 1982) and the spectroscopic coefficients $a_1$, $a_2$ (Liebe, 1983), and $a_3$ (Liebe et al., 1977) are listed in Table 1 for some 40 of these absorption lines.

Table 2 gives representative values of temperature and pressure at the high altitudes of interest here. They are taken from the U.S. Standard Atmosphere 76 (COESA, 1976) and are the values we shall assume throughout.

We note from Table 1 that most of the center frequencies are between 50 and 70 GHz. One exception is the $1^-$ line. It lies near 119 GHz, but we still include it as one of the lines of our study.

Also from Table 1 we note that the lines are generally separated by about 500 MHz. Since line widths above 30 km are 20 MHz or less, each line will be well isolated. Occassionally, however, the $K^+$ and $K^-$ lines happen to fall especially close, forming what are called "doublets." These doublets should probably be treated together. There are four of them and they are flagged in Table 1.

From (6) we observe that the imaginary part of SF(f) reaches its maximum of $S/\gamma$ at the center frequency. And from (7) and (8) we see that this ratio is independent of pressure. In addition, its dependence on temperature is not

Table 1. Line Frequencies and Coefficients for Microwave Transitions of $O_2$ in Air

| K± | $\nu_o$ | $a_1$ | $a_2$ | $a_3$ |
|---|---|---|---|---|
| | GHz | kHz/kPa $\times 10^{-6}$ | | GHz/kPa $\times 10^{-3}$ |
| 39- | 49.962257 | 0.34 | 10.724 | 8.50 |
| 37- | 50.474238 | 0.94 | 9.694 | 8.60 |
| 35- | 50.987749 | 2.46 | 8.694 | 8.70 |
| 33- | 51.503350 | 6.08 | 7.744 | 8.90 |
| 31- | 52.021410 | 14.14 | 6.844 | 9.20 |
| 29- | 52.542394 | 31.02 | 6.004 | 9.40 |
| 27- | 53.066907 | 64.10 | 5.224 | 9.70 |
| 25- | 53.595749 | 124.70 | 4.484 | 10.00 |
| 23- | 54.130000 | 228.00 | 3.814 | 10.20 |
| 21- | 54.671159 | 391.80 | 3.194 | 10.50 |
| 19- | 55.221367 | 631.60 | 2.624 | 10.79 |
| 17- | 55.783802 | 953.50 | 2.119 | 11.10 |
| 1+ \| | 56.264775 | 548.90 | 0.015 | 16.46 |
| 15- \| | 56.363389 | 1344.00 | 1.660 | 11.44 |
| 13- | 56.968206 | 1763.00 | 1.260 | 11.81 |
| 11- | 57.612484 | 2141.00 | 0.915 | 12.21 |
| 9- \| | 58.323877 | 2386.00 | 0.626 | 12.66 |
| 3+ \| | 58.446590 | 1457.00 | 0.084 | 14.49 |
| 7- | 59.164207 | 2404.00 | 0.391 | 13.19 |
| 5+ | 59.590983 | 2112.00 | 0.212 | 13.60 |
| 5- \| | 60.306061 | 2124.00 | 0.212 | 13.82 |
| 7+ \| | 60.434776 | 2461.00 | 0.391 | 12.97 |
| 9+ | 61.150560 | 2504.00 | 0.626 | 12.48 |
| 11+ | 61.800154 | 2298.00 | 0.915 | 12.07 |
| 13+ \| | 62.411215 | 1933.00 | 1.260 | 11.71 |
| 3- \| | 62.486260 | 1517.00 | 0.083 | 14.68 |
| 15+ | 62.997977 | 1503.00 | 1.665 | 11.39 |
| 17+ | 63.568518 | 1087.00 | 2.115 | 11.08 |
| 19+ | 64.127767 | 733.50 | 2.620 | 10.78 |
| 21+ | 64.678903 | 463.50 | 3.195 | 10.50 |
| 23+ | 65.224071 | 274.80 | 3.815 | 10.20 |
| 25+ | 65.764772 | 153.00 | 4.485 | 10.00 |
| 27+ | 66.302091 | 80.09 | 5.225 | 9.70 |
| 29+ | 66.836830 | 39.46 | 6.005 | 9.40 |
| 31+ | 67.369598 | 18.32 | 6.845 | 9.20 |
| 33+ | 67.900867 | 8.01 | 7.745 | 8.90 |
| 35+ | 68.431005 | 3.30 | 8.695 | 8.70 |
| 37+ | 68.960311 | 1.28 | 9.695 | 8.60 |
| 39+ | 69.489021 | 0.47 | 10.720 | 8.50 |
| 1- | 118.750343 | 945.00 | 0.009 | 16.30 |

Table 2. Temperature and Pressure in the Mesosphere
(U.S. Standard Atmosphere, 1976)

| Altitude | Atmosphere | Temperature | Pressure | Line Shape |
|---|---|---|---|---|
| km | | °C | Pa | |
| 30 | Stratosphere | -46.64 | 1197 | Lorentz |
| 35 | | -36.64 | 575 | |
| 40 | | -22.80 | 287 | |
| 45 | | - 8.99 | 149.1 | |
| 50 | Stratopause | - 2.50 | 79.8 | |
| 55 | | -12.38 | 42.5 | |
| 60 | Mesosphere | -26.13 | 22.0 | |
| 65 | | -39.86 | 10.93 | Voigt |
| 70 | | -53.56 | 5.22 | |
| 75 | | -64.75 | 2.39 | |
| 80 | | -74.51 | 1.14 | |
| 85 | Mesopause | -84.26 | 0.45 | |
| 90 | Thermosphere | -86.28 | 0.18 | |
| 95 | | -84.73 | 0.08 | Gauss |
| 100 | | -78.07 | 0.03 | |

great, and it follows that the absorption peaks are nearly independent of altitude. Actually, this is true only for fairly high pressures. As the pressure decreases to zero, the strength does continue to decrease, but the width is subject to a new phenomenon.

Formula (8) computes the "pressure-broadened" width. When it becomes very small, there are other broadening mechanisms that take over, the next of importance being Doppler broadening. This is associated with a "Gaussian" shape function and a line width equal to (with $\nu_o$ still in gigahertz)

$$\gamma_D = 1.096\ \nu_o \theta^{-1/2} \qquad \text{kHz.} \tag{9}$$

In the mesosphere it turns out that pressure-broadening and Doppler-broadening are of the same order of magnitude, and in place of either the Lorentz or Gauss functions, it is the intermediate Voigt line shape that theory will require. In Figure 1 are plotted examples of normalized Voigt profiles with both imaginary and real parts (u and v) shown. The Voigt function is hard to compute and following Olivero and Longbothum (1977) it seems an adequate

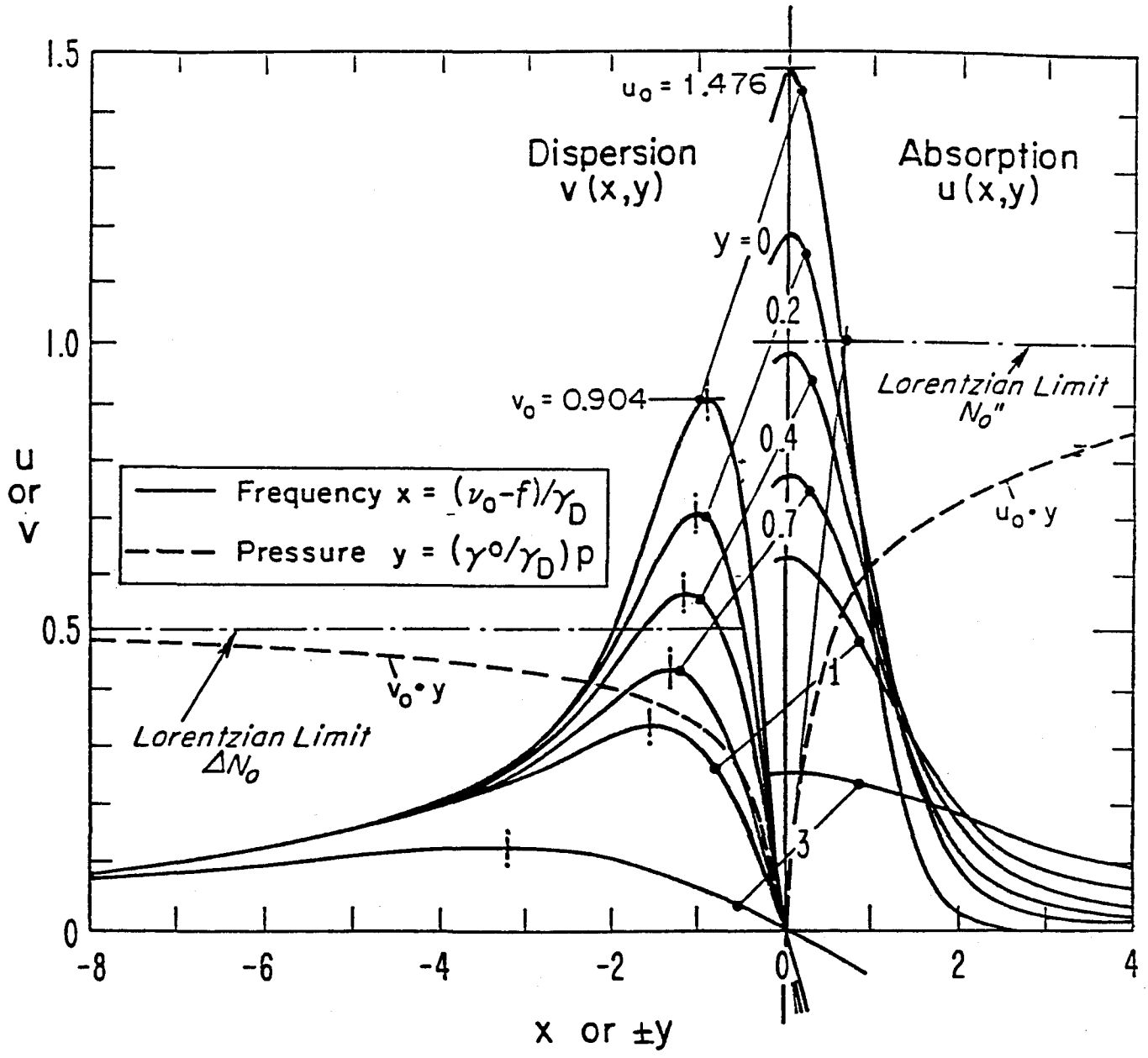


Figure 1. Normalized Voight profiles of absorption u and v. Shown are profiles versus frequency x at constant pressure y (solid curves) and the pressure profiles of maximum absorption $u_o$ and peak dispersion $v_o$.

approximation to retain the Lorentz shape function and to suppose that the $\gamma$ in (6) is replaced by

$$\gamma_h = 0.535\gamma + [(0.465\gamma)^2 + \gamma_D^2]^{1/2}. \qquad (10)$$

Our final model uses this last approximation with the Lorentz shape function. All told, it uses Table 1 and the formulas (5) through (10) to provide a spectrum of refractivity in the 60-GHz range under mesospheric conditions. Figure 2 shows plots of attenuation $\alpha$ and the dispersive part of the phase lag $\beta$ for the range from 50 to 70 GHz and for conditions at about 30 km altitude.

## 2.2 The Geomagnetic Field and the Zeeman Effect

The Zeeman effect occurs because each of the fine structure levels is degenerate since the corresponding states have undetermined azimuthal motion. If J is the quantum number of total angular momentum, then the quantum number M of azimuthal momentum can be any integer from -J to J. Thus the degeneracy is of order 2J + 1.

When, however, the oxygen molecule is subjected to a static magnetic field, there is a force acting on the internal magnetic dipole that causes the molecule to precess about the field. This precession affects the rotational energy in a manner directly related to the azimuthal quantum number M. The level then splits into 2J + 1 new levels, and this elimination of degeneracy is called the Zeeman effect.

For transitions between those many levels there are stringent selection rules. When J changes by one, we can simultaneously have M either remaining fixed or also changing by one. Furthermore, each of those transitions can arise because of interaction with only one component of the electromagnetic field. The line components obtained when M is unchanged are called the $\pi$ components and arise from interaction with a magnetic field vector that is linearly polarized in the direction of the static magnetic field. When M increases or decreases by one, the components are the $\sigma^+$ or $\sigma^-$ components and are caused by interacton with a magnetic field vector that is circularly polarized in the plane perpendicular to the static magnetic field. The $\sigma^+$ components arise from a right circularly polarized field and the $\sigma^-$ components from a left circularly polarized field. The convention used here is adapted

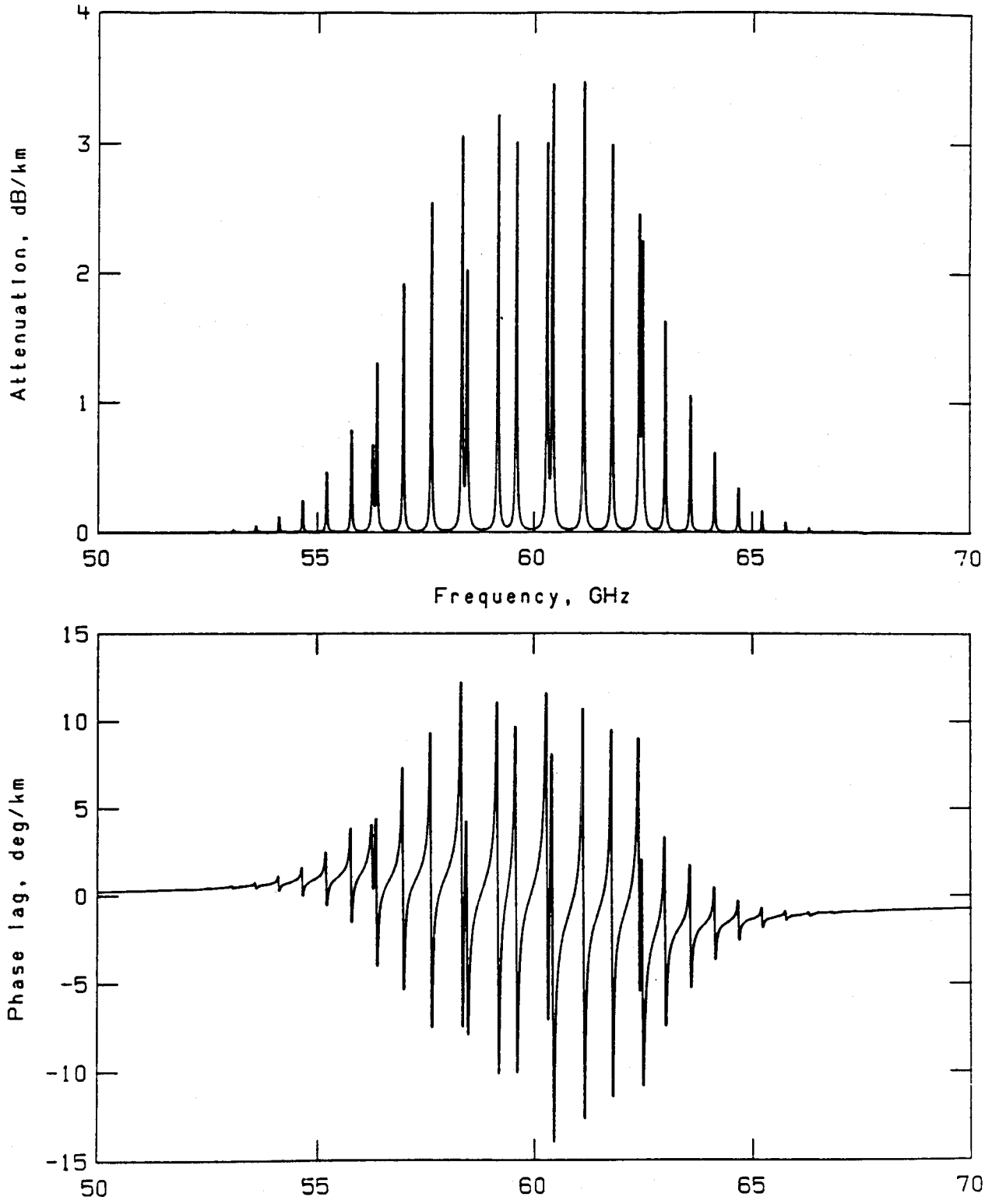


Figure 2. Pressure-broadened oxygen microwave lines in dry air for conditions at about 30 km altitude with p = w kPa, T = 225 K; at top is the attenuation spectrum and at bottom is the delay spectrum.

from the so-called IEEE convention and states that a right circularly polarized field rotates in the same direction as would a right-handed helix advancing in the direction (in this case) of the static magnetic field. That this anisotropic behavior is to be expected is suggested by noting that a force along the axis of rotation ought not to change the azimuthal motion while circularly polarized forces should do exactly that.

Figure 3 gives an example of the schematic distribution of energy levels and the allowed transitions for the case K = 3. A moment's look at this figure shows how each set of components of the $K^+$ line contains 2K + 1 sublines, while for the $K^-$ line each set contains 2K - 1 sublines.

The line center frequency of a single Zeeman component is given by

$$\nu_o^z = \nu_o + 28.03 \cdot 10^{-6}\ \eta\ B_o \quad \text{GHz}, \tag{11}$$

where $\nu_o$ is the center frequency of the unsplit line, $B_o$ (measured in microtesla) is the flux density of the static magnetic field, and $\eta$ is a coefficient that depends on J, K, M, and $\Delta M$. Since the geomagnetic field is on the order of 50 $\mu$T, it is large enough to spread the line by perhaps 3 MHz. In the mesosphere the magnetic field becomes an important part of the environment.

Each set of Zeeman components leads to a "refractivity" that is a function of frequency that we assume can be written as

$$N_\alpha(f) = \sum_M S\ \xi_M\ F_M(f), \tag{12}$$

where the functions F are the Lorentz shapes given in (6) and the center frequencies are in (11). The line strength S and the line width $\gamma$ (or $\gamma_h$) are independent of M and equal to the values given by (7) and (10). We speak of $N_o$ when the $\pi$ components are used and of $N_\pm$ for the $\sigma^\pm$ components.

A scheme to calculate the coefficients $\xi$ and $\eta$ for the individual Zeeman components was derived from the work of Lenoir (1968) by Liebe (1981) and is described in Table 3. Numerical and graphical results for the eight lines from $1^\pm$ to $7^\pm$ are illustrated in Table 4 and Figure 4. In addition, we note that $\Sigma\xi_M$ equals 1 in the case of $N_o$ and 1/2 for the other two. When $B_o = 0$ in (11) all the functions $F_M$ are equal and the terms in (12) add so that

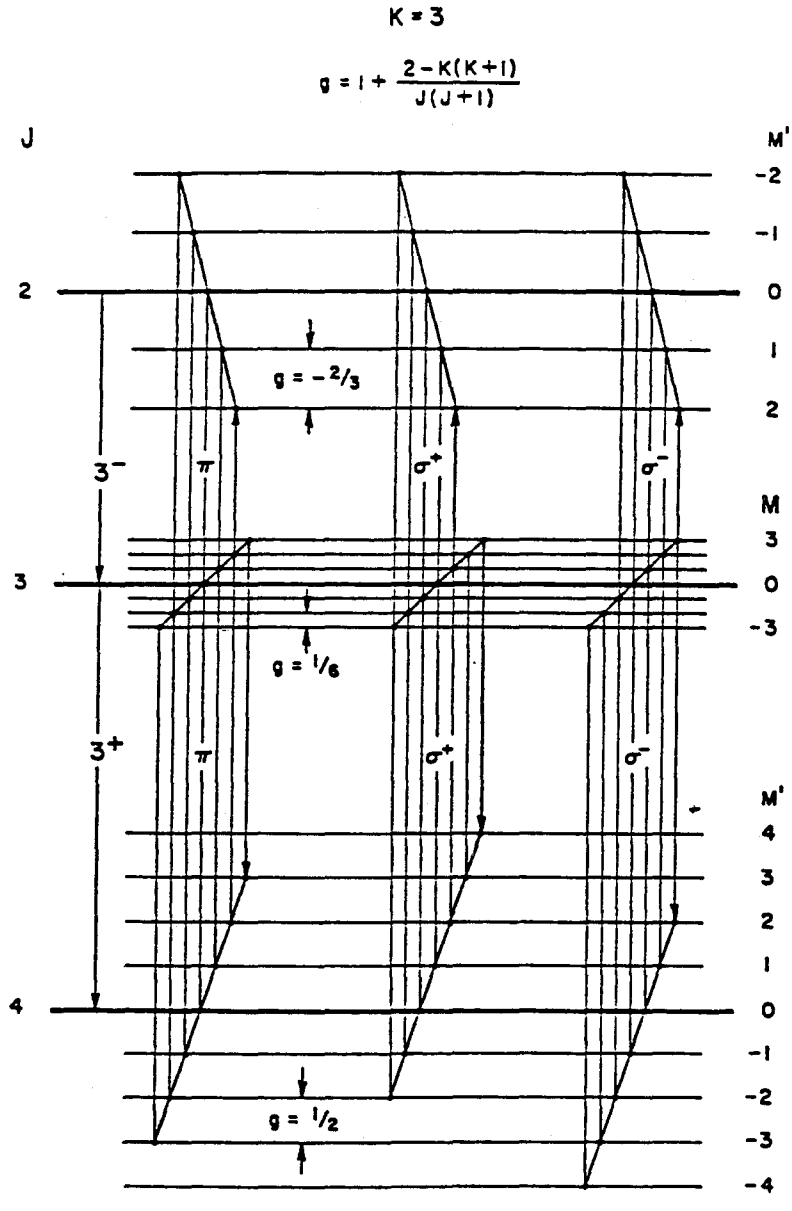


Figure 3. Schematic energy level diagram displaying the Zeeman components for the $3^+$ and $3^-$ oxygen microwave lines. In actuality, the energy levels for J = K±1 both lie below that for J = K.

Table 3. Coefficients for the Zeeman Components.

| Zeeman transitions | $\eta_M(K)$ | $\xi_M(K)$ | $\eta_M(K)$ | $\xi_M(K)$ |
|---|---|---|---|---|
| | $M=-K,-K+1,\ldots,K$ | | $M=-K+1,-K+2,\ldots,K-1$ | |
| $\pi$ $(\Delta M=0)$ | $\frac{M(K-1)}{K(K+1)}$ | $\frac{3((K+1)^2-M^2)}{(K+1)(2K+1)(2K+3)}$ | $\frac{M(K+2)}{K(K+1)}$ | $\frac{3(K^2-M^2)}{K(2K+1)(2K-1)}$ |
| $\sigma^+$ $(\Delta M=1)$ | $\frac{M(K-1)-K}{K(K+1)}$ | $\frac{3(K-M+1)(K-M+2)}{4(K+1)(2K+1)(2K+3)}$ | $\frac{M(K+2)-1}{K(K+1)}$ | $\frac{3(K-M+1)(K-M)}{4K(2K+1)(2K-1)}$ |
| $\sigma^-$ $(\Delta M=-1)$ | $\frac{M(K-1)+K}{K(K+1)}$ | $\frac{3(K+M+1)(K+M+2)}{4(K+1)(2K+1)(2K+3)}$ | $\frac{M(K+2)+1}{K(K+1)}$ | $\frac{3(K+M+1)(K+M)}{4K(2K+1)(2K-1)}$ |

$$2N_+ = 2N_- = N_o = N, \tag{13}$$

where N here is just the single line as previously defined in (5) and (6).

The three patterns of specific attenuation for the lines from $1^{\pm}$ to $29^{\pm}$ have been calculated for temperatures and pressures corresponding to heights ranging from 30 to 100 km and for the two geomagnetic flux densities of 30 and 60 $\mu$T. A catalog of the complete set was presented in graphical form by Liebe (1983). A sample consisting of the $7^+$ line is shown in Figure 5. We note that above 70 km the individual, now mostly Doppler-broadened, components become discernable, and that even at 40 km the three patterns are decidedly different, thus implying anisotropy.

We have referred to the three patterns as refractivities, but it is more exact to say they are components of the constitutive properties in the mesospheric atmosphere. Since it is the paramagnetic properties of oxygen that bring about the absorption lines, it is the magnetic permeability that is affected. To introduce the notation we shall use, we first note that in the usual isotropic case one expects the relative permeability to have the form

$$\mu_r = (1 + N)^2 \approx 1 + 2N,$$

where N is the refractivity and the approximation follows because N is on the order of $10^{-6}$. When the medium is anisotropic, the permeability becomes a tensor of rank 2 and we would expect to write

$$\mu = \mu_o(I + 2N), \tag{14}$$

Table 4. The Frequency Shifts η and Relative Intensity Factors ξ for the Zeeman Components of the 1± to 7± Oxygen Lines

| | K | $7^+$ | | $7^-$ | | $5^+$ | | $5^-$ | | $3^+$ | | $3^-$ | | $1^+$ | | $1^-$ | |
|---|---|---|---|---|---|---|---|---|---|---|---|---|---|---|---|---|---|
| | M | η | ξ | η | ξ | η | ξ | η | ξ | η | ξ | η | ξ | η | ξ | η | ξ |
| π | 7 | .7500 | .0221 | | | | | | | | | | | | | | |
| | 6 | .6429 | .0412 | .9643 | .0286 | | | | | | | | | | | | |
| | 5 | .5357 | .0574 | .8036 | .0527 | .6667 | .0385 | | | | | | | | | | |
| | 4 | .4286 | .0706 | .6429 | .0725 | .5333 | .0699 | .9333 | .0545 | | | | | | | | |
| | 3 | .3214 | .0809 | .4821 | .0879 | .4000 | .0944 | .7000 | .0970 | .5000 | .0833 | | | | | | |
| | 2 | .2143 | .0882 | .3214 | .0989 | .2667 | .1119 | .4667 | .1273 | .3333 | .1429 | .8333 | .1429 | | | | |
| | 1 | .1071 | .0926 | .1607 | .1055 | .1333 | .1224 | .2333 | .1455 | .1667 | .1786 | .4167 | .2286 | .0000 | .3000 | | |
| | 0 | .0000 | .0941 | .0000 | .1077 | .0000 | .1259 | .0000 | .1515 | .0000 | .1905 | .0000 | .2571 | .0000 | .4000 | .0000 | 1.0000 |
| | -1 | -.1071 | .0926 | -.1607 | .1055 | -.1333 | .1224 | -.2333 | .1455 | -.1667 | .1786 | -.4167 | .2286 | .0000 | .3000 | | |
| | -2 | -.2143 | .0882 | -.3214 | .0989 | -.2667 | .1119 | -.4667 | .1273 | -.3333 | .1429 | -.8333 | .1429 | | | | |
| | -3 | -.3214 | .0809 | -.4821 | .0879 | -.4000 | .0944 | -.7000 | .0970 | -.5000 | .0833 | | | | | | |
| | -4 | -.4286 | .0706 | -.6429 | .0725 | -.5333 | .0699 | -.9333 | .0545 | | | | | | | | |
| | -5 | -.5357 | .0574 | -.8036 | .0527 | -.6667 | .0385 | | | | | | | | | | |
| | -6 | -.6429 | .0412 | -.9643 | .0286 | | | | | | | | | | | | |
| | -7 | -.7500 | .0221 | | | | | | | | | | | | | | |
| $\sigma^+$ | 7 | .6250 | .0007 | | | | | | | | | | | | | | |
| | 6 | .5179 | .0022 | .9464 | .0011 | | | | | | | | | | | | |
| | 5 | .4107 | .0044 | .7857 | .0033 | .5000 | .0017 | | | | | | | | | | |
| | 4 | .3036 | .0074 | .6250 | .0066 | .3667 | .0052 | .9000 | .0030 | | | | | | | | |
| | 3 | .1964 | .0110 | .4643 | .0110 | .2333 | .0105 | .6667 | .0091 | .2500 | .0060 | | | | | | |
| | 2 | .0893 | .0154 | .3036 | .0165 | .1000 | .0175 | .4333 | .0182 | .0833 | .0179 | .7500 | .0143 | | | | |
| | 1 | -.0179 | .0206 | .1429 | .0231 | -.0333 | .0262 | .2000 | .0303 | -.0833 | .0357 | .3333 | .0429 | -.5000 | .0500 | | |
| | 0 | -.1250 | .0265 | -.0179 | .0308 | -.1667 | .0367 | -.0333 | .0455 | -.2500 | .0595 | -.0833 | .0857 | -.5000 | .1500 | -.5000 | .5000 |
| | -1 | -.2321 | .0331 | -.1786 | .0396 | -.3000 | .0490 | -.2667 | .0636 | -.4167 | .0893 | -.5000 | .1429 | -.5000 | .3000 | | |
| | -2 | -.3393 | .0404 | -.3393 | .0495 | -.4333 | .0629 | -.5000 | .0848 | -.5833 | .1250 | -.9167 | .2143 | | | | |
| | -3 | -.4464 | .0485 | -.5000 | .0604 | -.5667 | .0787 | -.7333 | .1091 | -.7500 | .1667 | | | | | | |
| | -4 | -.5536 | .0574 | -.6607 | .0725 | -.7000 | .0962 | -.9667 | .1364 | | | | | | | | |
| | -5 | -.6607 | .0669 | -.8214 | .0857 | -.8333 | .1154 | | | | | | | | | | |
| | -6 | -.7679 | .0772 | -.9821 | .1000 | | | | | | | | | | | | |
| | -7 | -.8750 | .0882 | | | | | | | | | | | | | | |
| $\sigma^-$ | 7 | .8750 | .0882 | | | | | | | | | | | | | | |
| | 6 | .7679 | .0772 | .9821 | .1000 | | | | | | | | | | | | |
| | 5 | .6607 | .0669 | .8214 | .0857 | .8333 | .1154 | | | | | | | | | | |
| | 4 | .5536 | .0574 | .6607 | .0725 | .7000 | .0962 | .9667 | .1364 | | | | | | | | |
| | 3 | .4464 | .0485 | .5000 | .0604 | .5667 | .0787 | .7333 | .1091 | .7500 | .1667 | | | | | | |
| | 2 | .3393 | .0404 | .3393 | .0495 | .4333 | .0629 | .5000 | .0848 | .5833 | .1250 | .9167 | .2143 | | | | |
| | 1 | .2321 | .0331 | .1786 | .0396 | .3000 | .0490 | .2667 | .0636 | .4167 | .0893 | .5000 | .1429 | .5000 | .3000 | | |
| | 0 | .1250 | .0265 | .0179 | .0308 | .1667 | .0367 | .0333 | .0455 | .2500 | .0595 | .0833 | .0857 | .5000 | .1500 | .5000 | .5000 |
| | -1 | .0179 | .0206 | -.1429 | .0231 | .0333 | .0262 | -.2000 | .0303 | .0833 | .0357 | -.3333 | .0429 | .5000 | .0500 | | |
| | -2 | -.0893 | .0154 | -.3036 | .0165 | -.1000 | .0175 | -.4333 | .0182 | -.0833 | .0179 | -.7500 | .0143 | | | | |
| | -3 | -.1964 | .0110 | -.4643 | .0110 | -.2333 | .0105 | -.6667 | .0091 | -.2500 | .0060 | | | | | | |
| | -4 | -.3036 | .0074 | -.6250 | .0066 | -.3667 | .0052 | -.9000 | .0030 | | | | | | | | |
| | -5 | -.4107 | .0044 | -.7857 | .0033 | -.5000 | .0017 | | | | | | | | | | |
| | -6 | -.5179 | .0022 | -.9464 | .0011 | | | | | | | | | | | | |
| | -7 | -.6250 | .0007 | | | | | | | | | | | | | | |

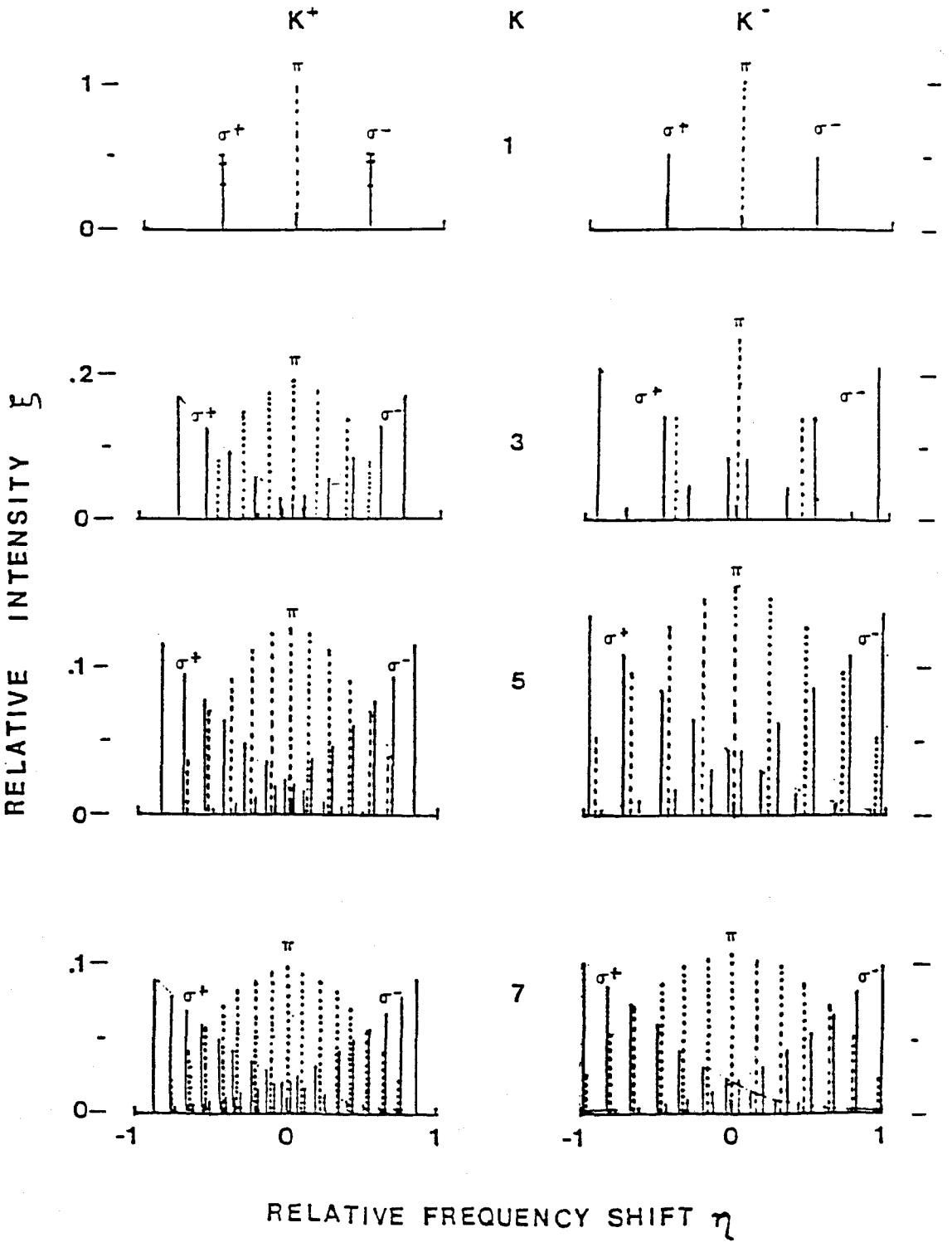


Figure 4. Schematic plots of the frequency shifts $\eta$ and relative intensity factors $\xi$ for the Zeeman components of the $1^{\pm}$ to $7^{\pm}$ oxygen lines.

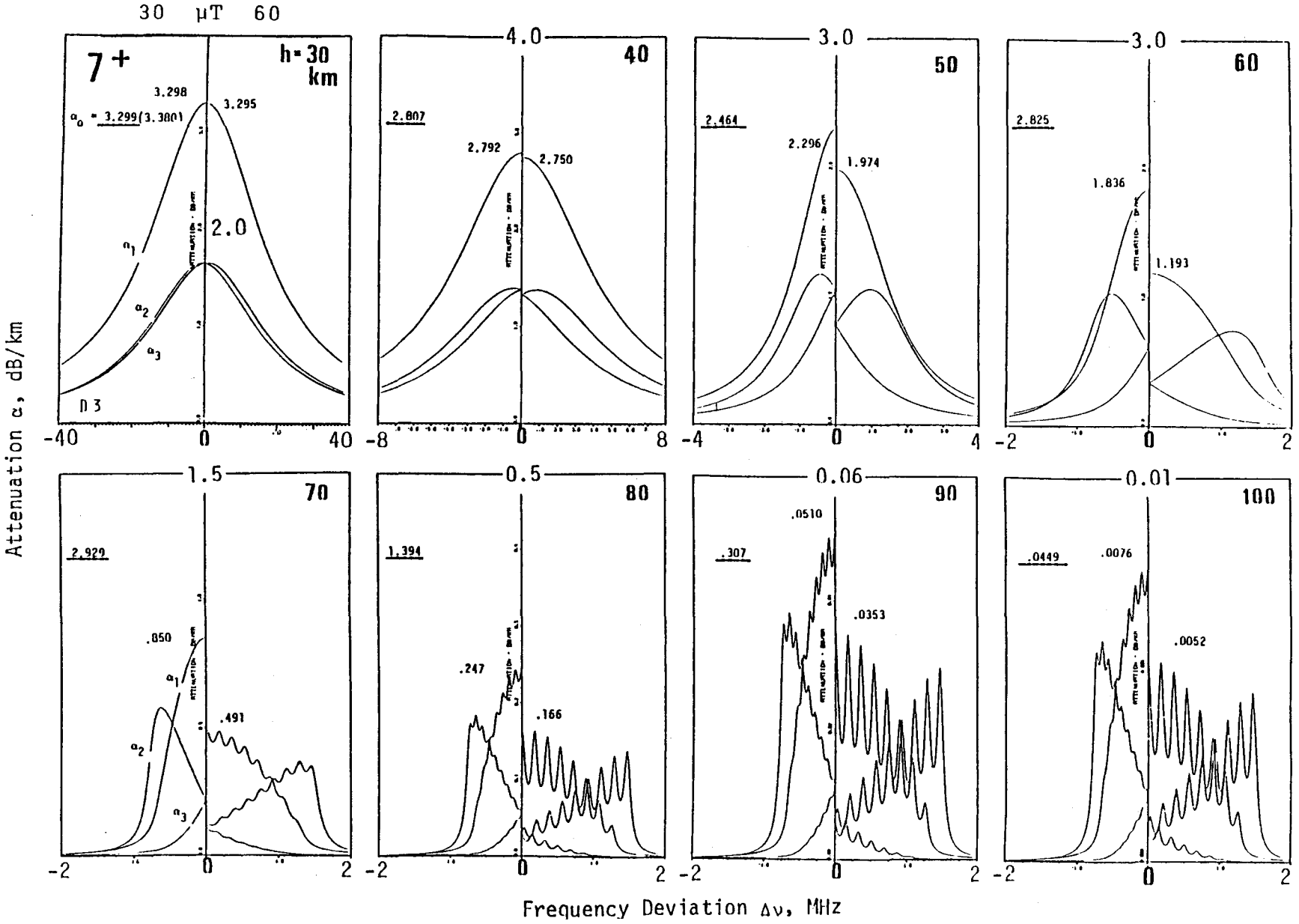


Figure 5. Attenuation patterns of the $7^+$ oxygen line for altitudes from 30 to 100 km. Each frame displays the three separate patterns for magnetic flux densities of 30 and 60 $\mu$T.

where $\mu_o = 4\pi \cdot 10^{-7}$ H/m is the permeability of free space, **I** is the unit tensor, and **N** would be a kind of refractivity tensor.

We can represent **N** as a 3x3 matrix once we specify a coordinate system. Let $\mathbf{e}_o$ be a unit vector in the direction of the geomagnetic field, and let $\mathbf{e}_r$, $\mathbf{e}_\ell$ be vectors of unit size that represent right and left circularly polarized fields in the plane orthogonal to $\mathbf{e}_o$. Then in terms of the basis $(\mathbf{e}_r, \mathbf{e}_\ell, \mathbf{e}_o)$ the tensor **N** is represented by the diagonal matrix

$$\mathbf{N} = \begin{bmatrix} 2N_+ & 0 & 0 \\ 0 & 2N_- & 0 \\ 0 & 0 & N_o \end{bmatrix} \tag{15}$$

Turning to more customary notation, let us use the basis $(\mathbf{e}_x, \mathbf{e}_y, \mathbf{e}_o)$ where $\mathbf{e}_x$, $\mathbf{e}_y$ are real unit vectors that combine with $\mathbf{e}_o$ to form a right-handed orthogonal triad. We may write

$$\mathbf{e}_r = (\mathbf{e}_x + i\mathbf{e}_y)/\sqrt{2} \quad \text{and} \quad \mathbf{e}_\ell = (\mathbf{e}_x - i\mathbf{e}_y)/\sqrt{2}\ , \tag{16}$$

so that the transformation from the first circular components to the new linear ones is

$$\mathbf{C} = \begin{bmatrix} 1/\sqrt{2} & 1/\sqrt{2} & 0 \\ i/\sqrt{2} & -i/\sqrt{2} & 0 \\ 0 & 0 & 1 \end{bmatrix} \tag{17}$$

The refractivity tensor can now be represented by the matrix obtained through a "similarity transformation,"

$$\mathbf{N}' = \mathbf{C}\,\mathbf{N}\,\mathbf{C}^{-1} = \begin{bmatrix} N_+ + N_- & -i(N_+ - N_-) & 0 \\ i(N_+ - N_-) & N_+ + N_- & 0 \\ 0 & 0 & N_o \end{bmatrix} \tag{18}$$

where we use the conventional prime for the matrix representation in the "new coordinate system." Note that when the magnetic field $B_o$ decreases to zero, it follows from (13) that both matrices (15) and (18) reduce to a simple refractivity times the unit matrix.

## 3. RADIO WAVE PROPAGATION IN THE ANISOTROPIC MESOSPHERE

The previous section has shown how to describe the pertinent properties of the mesosphere. We now turn to a study of how these properties affect the propagation of radio waves. Some matrix theory is involved here, most of which may be found in texts such as that of Courant and Hilbert (1953).

### 3.1 Basic Equations for Plane-Wave Propagation

Because we seem required to treat an anisotropic medium, we shall proceed with some caution and begin with Maxwell's equations

$$\nabla \times \mathbf{H} = -i\omega\mathbf{D} \qquad \text{and} \qquad \nabla \times \mathbf{E} = i\omega\mathbf{B}, \tag{19}$$

where $\omega = 2\pi f$ is the radial frequency. As we have seen in the previous section, the constitutive equations will take the form

$$\mathbf{D} = \epsilon_o\mathbf{E} \qquad \text{and} \qquad \mathbf{B} = \mu_o(\mathbf{I} + 2\mathbf{N})\mathbf{H} \tag{20}$$

so that it is the introduction of the tensor $\mathbf{N}$ that is unfamiliar. If desired, one can include the nondispersive part of the refractivity given in (1) as either part of the electric permittivity or as a further part of the permeability.

We look for a plane wave solution to (19) and (20). We suppose a Cartesian coordinate system (not that of the previous section) oriented so that all the vector fields vary only in the z-coordinate, thus representing a wave traveling in the direction of the z-axis. Then (19) assumes the form of the six simultaneous equations

$$\begin{aligned} -dH_y/dz &= -i\omega\epsilon_o E_x, & -dE_y/dz &= i\omega B_x, \\ dH_x/dz &= -i\omega\epsilon_o E_y, & dE_x/dz &= i\omega B_y, \\ 0 &= -i\omega\epsilon_o E_z, & 0 &= i\omega B_z. \end{aligned} \tag{21}$$

On the left sides we have derivatives of $\mathbf{H}$ and $\mathbf{E}$ and on the right sides are linear combinations of the same vectors. Thus the standard methods for solving sets of linear differential equations should be applicable here.

The equations in the last row of (21) are only algebraic. They say that $E_z$ and $B_z$ vanish so that the vectors $\mathbf{E}$ and $\mathbf{B}$ lie wholly in the xy-plane

perpendicular to the direction of propagation. The same is not true, however, of the vector **H**. Using (20), the equation $B_z = 0$ can be written

$$2N_{zx}H_x + 2N_{zy}H_y + (1 + 2N_{zz})H_z = 0, \tag{22}$$

where $N_{zx}, \ldots$ are elements of the matrix representing **N**. Then (22) can be solved for $H_z$ and is generally not zero.

Differentiating the first column of (21) and using the second column, we find

$$d^2H_x/dz^2 = -(k^2/\mu_o)B_x \qquad \text{and} \qquad d^2H_y/dz^2 = -(k^2/\mu_o)B_y, \tag{23}$$

since $k^2 = \omega^2\epsilon_o\mu_o$. Because of (20) the functions $B_x$, $B_y$ may be expressed as linear combinations of the three components of **H**. We solve (22) for $H_z$ and replace its appearance in (23) by this solution. In this way $B_x$, $B_y$ will become linear combinations of the two unknowns $H_x$, $H_y$.

Actually, because **N** is small we may shorten this suggested process. The solution to (22) has the variables $H_x$, $H_y$ multiplied by coefficients of the order of N, and the appearances of $H_z$ in (23) also have coefficients of this order. Thus $H_z$, while not zero, is small, and if the above process is carried out the coefficients of $H_x$, $H_y$ in (23) are changed by something on the order of $N^2$. We therefore ignore the terms involving $H_z$ in (23) and so write

$$d^2\mathbf{H}/dz^2 = -k^2(\mathbf{I} + 2\mathbf{N}^m)\mathbf{H}, \tag{24}$$

where **H** is now a two-dimensional vector in the xy-plane, and $\mathbf{N}^m$ is the 2x2 submatrix of **N** obtained by discarding the last column and the last row.

A trial solution to (24) might take the form

$$\mathbf{H}(z) = \exp(ikz\mathbf{G})\mathbf{H}_o, \tag{25}$$

where $\mathbf{H}_o$ would be an "initial value" (when z = 0) of **H**, **G** is a 2x2 matrix whose value we seek, and where we do indeed mean to take the exponential of that matrix. This exponential is to be defined in the standard way using either the infinite power series or the properties of differentiation. It will follow that (25) satisfies (24) provided

$$\mathbf{G}^2 = \mathbf{I} + 2\mathbf{N}^m \tag{26}$$

or, in other words, provided **G** is a square root of the right-hand side. The most obvious square root has the simple approximation

$$\mathbf{G} = \mathbf{I} + \mathbf{N}^m \tag{27}$$

with an error again on the order of $N^2$. Substituting (27) in (25) we have the final result

$$\mathbf{H}(z) = \exp[ikz(\mathbf{I} + \mathbf{N}^m)]\mathbf{H}_o. \tag{28}$$

There are, of course, other solutions to (24), for to identify a unique solution to a second-order differential equation it is necessary also to specify an initial first derivative. Such additional solutions are derived from other square roots in (26) and have to do with waves traveling in the negative z-direction.

One final detail here concerns how to calculate the electric field vector **E**. From the first column of (21) and from (28) we find

$$\mathbf{E} = (i/\omega\epsilon_o)\ \mathbf{e}_z \times d\mathbf{H}/dz = -Z_o\ \mathbf{e}_z \times (\mathbf{I} + \mathbf{N}^m)\mathbf{H}, \tag{29}$$

where $Z_o$ is the intrinsic impedance of free space and $\mathbf{e}_z$ is the unit vector in the direction of propagation. Note that **E** is not orthogonal to **H** but that the discrepancy is only of order N.

In (28), the appearance of **N** is in the exponent and is multiplied by the very large number kz. It can, therefore, have a strong effect on radio propagation. In (29), however, its appearance has a constant relation to the rest of the expression. It can be ignored, leaving us with the usual formula

$$\mathbf{E} = -\ Z_o\ \mathbf{e}_z \times \mathbf{H}. \tag{30}$$

### 3.2 The Refractivity Matrix

In Section 2.2, we saw how the refractivity tensor **N** could be represented as a 3x3 matrix. We now need a representation for $\mathbf{N}^m$. Another way of writing (18) is to separate out the component parts so that

$$\mathbf{N} = N_o \mathbf{P}_o + 2N_+ \mathbf{P}_+ + 2N_- \mathbf{P}_- \tag{31}$$

where, using the previously defined basis vectors $\mathbf{e}_x$, $\mathbf{e}_y$, $\mathbf{e}_o$,

$$\mathbf{P}_o = \begin{bmatrix} 0 & 0 & 0 \\ 0 & 0 & 0 \\ 0 & 0 & 1 \end{bmatrix} \quad \text{and} \quad \mathbf{P}_\pm = (1/2) \begin{bmatrix} 1 & \mp i & 0 \\ \pm i & 1 & 0 \\ 0 & 0 & 0 \end{bmatrix} \tag{32}$$

These $\mathbf{P}_\alpha$ are orthogonal projections onto the three eigenspaces that correspond to linear polarization in the direction of the geomagnetic field and the two orthogonal circular polarizations. The expression in (31) is called the "spectral decomposition" of the tensor operator **N**. Note, however, that despite its appearance, **N** is not Hermitean symmetric. The eigenvalues $N_o$, $2N_\pm$ are complex-valued and this destroys many of the properties one usually associates with similar entities.

The tensor **N** depends for its definition on the special vector $\mathbf{e}_o$, the unit vector in the direction of the geomagnetic field and the analysis in Section 3.1 introduced a second special vector $\mathbf{e}_z$, the unit vector in the direction of propagation. In both cases the x- and y-coordinates were perpendicular to the respective special directions but were otherwise arbitrary. To fix them, we now suppose that $\mathbf{e}_x$ is the unit vector in the direction of $\mathbf{e}_z \times \mathbf{e}_o$. Thus it is perpendicular to both longitudinal vectors. There will be two different y-coordinates that complete the respective right handed Cartesian coordinate systems.

In this way, we have constructed an "old" coordinate system with basis $(\mathbf{e}_x, \mathbf{e}_y, \mathbf{e}_o)$ in which **N** is represented as in (18) or (31); and we have a "new" system with basis $(\mathbf{e}_x, \mathbf{e}_y', \mathbf{e}_z)$ in which we want to represent **N**. Let $\phi$ be the angle between the geomagnetic field and the direction of propagation--between $\mathbf{e}_o$ and $\mathbf{e}_z$. Then the rotation matrix, which gives the new coordinates in terms of the old, is

$$\mathbf{R} = \begin{bmatrix} 1 & 0 & 0 \\ 0 & \cos\phi & -\sin\phi \\ 0 & \sin\phi & \cos\phi \end{bmatrix} \tag{33}$$

and similarity transformations provide new representations of the projections $P_\alpha$:

$$P_o' = R\,P_o\,R^{-1} = \begin{bmatrix} 0 & 0 & 0 \\ 0 & \sin^2\phi & \sin\phi\cos\phi \\ 0 & \sin\phi\cos\phi & \cos^2\phi \end{bmatrix}$$

$$P_\pm' = R\,P_\pm\,R^{-1} = 1/2 \begin{bmatrix} 1 & \mp i\cos\phi & \pm i\sin\phi \\ \pm i\cos\phi & \cos^2\phi & -\sin\phi\cos\phi \\ \mp i\sin\phi & -\sin\phi\cos\phi & \sin^2\phi \end{bmatrix} \tag{34}$$

A corresponding representation for **N** follows from (31).

To complete the process of Section 3.1, we simply discard the third rows and third columns in the matrices of (34) to obtain the 2x2 matrices

$$Q_o^m = \begin{bmatrix} 0 & 0 \\ 0 & \sin^2\phi \end{bmatrix}, \qquad Q_\pm^m = 1/2 \begin{bmatrix} 1 & \mp i\cos\phi \\ \pm i\cos\phi & \cos^2\phi \end{bmatrix} \tag{35}$$

whence

$$\mathbf{N}^m = N_o Q_o^m + 2N_+ Q_+^m + 2N_- Q_-^m = \begin{bmatrix} N_+ + N_- & -i(N_+ - N_-)\cos\phi \\ i(N_+ - N_-)\cos\phi & N_o\sin^2\phi + (N_+ + N_-)\cos^2\phi \end{bmatrix} \tag{36}$$

Until now, we have treated the refractivity and its effects as associated with the magnetic H-vector. This is the physically natural approach, but it is probably not entirely satisfying to the engineer. To change to a direct analysis of the electric E-vector, we note that (30) refers to two-dimensional vectors in the xy-plane perpendicular to the direction of propagation and can be rewritten as

$$E = -Z_o\,K\,H \tag{37}$$

where **K** is the 2x2 matrix

$$K = \begin{bmatrix} 0 & -1 \\ 1 & 0 \end{bmatrix} \tag{38}$$

We apply a similarity transformation to obtain

$$\mathbf{N}^e = \mathbf{K}\,\mathbf{N}^m\,\mathbf{K}^{-1} = \begin{bmatrix} N_o\sin^2\phi + (N_+ + N_-)\cos^2\phi & -i(N_+ - N_-)\cos\phi \\ i(N_+ + N_-)\cos\phi & N_+ + N_- \end{bmatrix} \tag{39}$$

and then the plane wave E-vector is given by

$$E(z) = \exp[ikz(I + \mathbf{N}^e)]\; E_o, \tag{40}$$

where $E_o$ is the initial value.

### 3.3 Characteristic Waves

The computation of the exponential in (28) or (40) may be carried out using any of several techniques (see, e.g., Moler and Van Loan, 1978). For example, we could use the standard series expression to write

$$\exp(s\mathbf{A}) = \mathbf{I} + (s/1!)\mathbf{A} + (s^2/2!)\mathbf{A}^2 + \ldots \tag{41}$$

for any complex number s and any square matrix **A**. Although this series always converges, the calculations are tedious and subject to round-off error.

Another technique involves the spectral decomposition of the matrix. It provides a physical insight that other methods lack, and it involves fairly easy and usually robust computations. We first look for complex numbers $\rho$ (the "eigenvalues") and vectors **v** (the "corresponding eigenvectors"), which satisfy

$$\mathbf{A}\,\mathbf{v} = \rho\mathbf{v}\ . \tag{42}$$

It will follow that

$$\mathbf{A}^n\mathbf{v} = \rho^n\mathbf{v} \tag{43}$$

and

$$\exp(s\mathbf{A})\mathbf{v} = \exp(s\rho)\mathbf{v}\ . \tag{44}$$

Thus, it is easy to compute how the exponential acts on these special vectors. To find how it acts on some other vector, one expands it into a linear combination of the eigenvectors and then applies (44) to each term.

In particular, consider the matrix $\mathbf{N}^e$. To solve the equivalent of (42) we first treat the scalar equation (the "characteristic equation")

$$\det(\rho \mathbf{I} - \mathbf{N}^e) = 0 \quad . \tag{45}$$

Since these are 2x2 matrices, this equation is quadratic in $\rho$ and there should be two solutions $\rho_1$ and $\rho_2$. Given these numbers, it is fairly easy to find the corresponding eigenvectors $\mathbf{v}_1$ and $\mathbf{v}_2$ and then (40) becomes

$$\mathbf{v}_j(z) = \exp[ikz(1 + \rho_j)]\ \mathbf{v}_j \quad , \qquad j = 1,\ 2 \tag{46}$$

whenever the initial field equals an eigenvector. The vector functions $\mathbf{v}_j(z)$ are plane wave solutions to the original Maxwell's equations. They are called *characteristic waves* and they have the property that, while they may change in size and phase, they always retain their original appearance and orientation.

The two eigenvectors are linearly independent and for any initial field we may find complex numbers $E_1$ and $E_2$, so that

$$E_o = E_1\ \mathbf{v}_1 + E_2\ \mathbf{v}_2 \quad . \tag{47}$$

Then the exponential in (40) quickly becomes

$$E(z) = e^{ikz}[E_1 \exp(ikz\rho_1)\ \mathbf{v}_1 + E_2 \exp(ikz\rho_2)\ \mathbf{v}_2] \ , \tag{48}$$

so that the propagating vector field is now represented as a linear combination of the two characteristic waves.

As a general rule the eigenvalues $\rho_j$ have the same order of magnitude as N and have positive imaginary parts so that as z increases, E(z) decreases exponentially. Generally these imaginary parts differ, so that one of the two components in (48) decreases faster than the other. After some distance, it becomes relatively small and E(z) approaches the appearance of the other, more dominant characteristic wave.

It will probably also be true that the real parts of the eigenvalues differ. The two characteristic waves travel at different speeds and the phase relation between the two components in (48) varies continuously. What this usually means is that the ellipse of polarization appears to rotate in space as the wave progresses, thus exhibiting a "Faraday rotation."

There are several aids that may be used to compute eigenvalues and eigenvectors. For example, we have

$$\rho_1\rho_2 = \det(\mathbf{N}^e) = 4N_+N_-\cos^2\phi + N_o(N_+ + N_-)\sin^2\phi$$

and (49)

$$\rho_1 + \rho_2 = \mathrm{trace}(\mathbf{N}^e) = 2(N_+ + N_-) + (N_o - N_+ - N_-)\sin^2\phi \ ,$$

from which the two $\rho_j$ may be found. Let us suppose that $\rho$ is one of these two and that we seek the corresponding eigenvector $\mathbf{v}$. We suppose its components have the values $v_x$, $v_y$, so that the equation $\mathbf{N}^e\mathbf{v} = \rho\mathbf{v}$ becomes a set of two equations in these two unknowns. The second of these equations is

$$i(N_+ - N_-)\cos\phi\ v_x + (N_+ + N_-)v_y = \rho v_y \tag{50}$$

and one solution is

$$v_x = \rho - N_+ - N_- \qquad \text{and} \qquad v_y = i(N_+ - N_-)\cos\phi \ . \tag{51}$$

Since $\rho$ is an eigenvalue, it is guaranteed that the first equation is also satisfied. Of course, any scalar multiple of (51) will also be an eigenvector and the usual practice is to normalize so it has unit size.

There remains the problem of finding the numbers $E_1$, $E_2$ of (47). For this purpose, it should be pointed out that the two eigenvectors are usually not orthogonal. Because the $N_\alpha$ are complex-valued, the matrix $\mathbf{N}^e$ is not Hermitean symmetric and the usual theorems do not apply. It is best to simply treat (47) as two equations in the two unknowns and to employ a straightforward approach for the solutions.

A case of special interest occurs when $\phi = 0$. The solutions to (49) are $2N_+$ and $2N_-$, and when these are inserted into (51) we find the corresponding eigenvectors are, respectively, right circularly polarized and left circularly

polarized. This agrees with (15) and this is because the direction of propagation is along the geomagnetic field.

When $\phi = \pi/2$, the eigenvalues are $N_o$ and $N_+ + N_-$, and the corresponding eigenvectors are linearly polarized with the E-vector pointing respectively along the x-axis and along the y-axis. For the first of these, the H-vector points along the y-axis which, we note, is now the direction of the geomagnetic field.

### 3.4 Polarization and Stokes Parameters

We have seen how the polarization of a field vector may change as it propagates through this medium. To describe this change and its engineering consequences, we need to be able to describe the polarization in a quantitative way.

When our analyses concern a complex field such as E, we are, of course, using a shorthand notation for something like $Re[\exp(i2\pi ft)E]$. As time increases through one cycle, this latter real vector describes an ellipse, which is then the "ellipse of polarization." An obvious way to describe that ellipse is to measure both its ellipticity and the angle its major axis makes with some reference direction and, perhaps, an indication of the sense of rotation around the ellipse. In degenerate cases, one speaks qualitatively of linear polarization and of right and left circular polarization.

One standard and universally applicable way to measure polarization is through the use of what are called the *Stokes parameters*. These are discussed in many texts (see e. g., Born and Wolf, 1959, especially Section 1.4); here we shall try only to summarize some of their attributes.

As in Section 3.2, let **E** lie in the x,y-plane and let $E_x$, $E_y$ be the complex-valued components. Then the four Stokes parameters, $g_o$, $g_1$, $g_2$, $g_3$, are real numbers given by

$$\begin{aligned} g_o &= |E_x|^2 + |E_y|^2 \\ g_1 &= |E_x|^2 - |E_y|^2 \\ g_2 &= 2\, Re[E_x^*\, E_y] \\ g_3 &= 2\, Im[E_x^*\, E_y] \end{aligned} \tag{52}$$

or, in more compact form,

$$g_2 + ig_3 = 2\, E_x^*\, E_y,$$

where the star has been used to indicate the complex conjugate.

We first note that $g_o$ is positive and equals the total field strength. Then also we quickly find

$$g_o^2 = g_1^2 + g_2^2 + g_3^2 \quad , \tag{53}$$

so that in a three-dimensional space with $g_1$, $g_2$, $g_3$ axes, the Stokes parameters of a field vector lie on the surface of a sphere of radius $g_o$. This is the *Poincaré sphere* and provides an attractive geometric picture of the situation.

Given the Stokes parameters, we can write

$$\begin{aligned} E_x &= [(g_o + g_1)/2]^{\frac{1}{2}} \exp(i\psi) \quad , \\ E_y &= [2(g_o + g_1)]^{-\frac{1}{2}}(g_2 + ig_3) \exp(i\psi) \quad , \end{aligned} \tag{54}$$

where $\psi$ is an arbitrary phase angle. Thus not only does the vector E determine the Stokes parameters but also they in turn determine the vector--up to within that arbitrary phase angle. Since the absolute phase of the field is probably not measurable, the Stokes parameters seem to represent all the useful information for the field.

What relates the parameters directly to the ellipse of polarization is the representation of the Poincaré sphere in spherical coordinates

$$\begin{aligned} g_1 &= g_o \cos 2\tau \cos 2\delta \quad , \\ g_2 &= g_o \cos 2\tau \sin 2\delta \quad , \\ g_3 &= g_o \sin 2\tau \quad . \end{aligned} \tag{55}$$

It turns out that $\delta$ $(0 \leq \delta < \pi)$ is the angle between the major axis of the ellipse and the x-axis, while $\tan \tau = \pm b/a$ $(-\pi/4 \leq \tau \leq \pi/4)$, where a and b are the major and minor semiaxes and the sign is chosen according to the sense of rotation. On the sphere, then, the azimuth measures the tilt of the field while the declination measures the ellipticity.

Thus the four Stokes parameters provide the total field strength and a complete description of the polarization. Often, however, one wants to describe only the polarization, and for this one can use the "normalized Stokes parameters." These are obtained by normalizing the vector E so it has unit size or more directly by dividing all parameters by $g_o$. For the

normalized Stokes parameters, $g_o$ is always 1 and the Poincaré sphere has unit radius. Treating this sphere as a globe, one sees immediately that the northern hemisphere and the North Pole correspond to right-hand polarization and right circular polarization, while the southern hemisphere and the South Pole correspond to left-hand polarization and to left circular polarization. The Equator corresponds to linear polarization with the "East Pole" at $(g_1,g_2,g_3) = (1,0,0)$ corresponding to polarization along the x-axis and $(-1,0,0)$ to polarization along the y-axis.

If **E** represents the electric field vector at the aperture of a receiving antenna, then we expect the voltage V at the antenna terminals to be a linear function of **E**. We may write

$$V = G\ \mathbf{E}\cdot\mathbf{P}^* \tag{56}$$

where G is the (voltage) gain of the antenna and **P** is a complex vector of unit size in the x,y-plane that would be called the "polarization of the antenna." For the two vectors **E**, **P** we can find the respective normalized Stokes parameters and plot them on the Poincaré sphere. It then turns out that

$$|V| = G\ |\mathbf{E}|\ \cos(\Delta/2)\quad , \tag{57}$$

where $\Delta$ is the angle between the two plotted points. Thus maximum efficiency of reception occurs when **E** and **P** differ by only a multiplicative scalar, and V becomes 0 (the two vectors are "orthogonal") when they appear at opposite points on the Poincaré sphere.

There is an alternative way to measure polarization that has been especially championed by Beckmann (1968). Given the components $E_x$, $E_y$ as before, one defines the complex number

$$p = E_y/E_x\ . \tag{58}$$

From (54) we have immediately

$$p = (g_2 + ig_3)/(g_o + g_1) \tag{59}$$

and, when the Stokes parameters are normalized,

$$g_1 = (1 - |p|^2)/(1 + |p|^2) , \qquad g_2 + ig_3 = 2p/(1 + |p|^2) . \tag{60}$$

Thus, the one complex number p provides the same information as the three real normalized Stokes parameters. In particular, the real p-axis corresponds to linear polarization, the upper half-plane to right-hand polarization, and the lower half-plane to left-hand polarization. The point p = i corresponds to right circular polarization, p = -i to left circular polarization, p = 0 to linear polarization along the x-axis, and p = ∞ to linear polarization along the y-axis.

The advantage of Beckmann's notation is its simplicity and the fact that this seemingly complicated subject has been reduced to single number. The disadvantage is a certain loss of symmetry between small values of p (near where $g_1 = 1$) and large values (near $g_1 = -1$). Indeed, the fact that we need to introduce the point at infinity shows that we are really using the Riemann sphere of complex numbers; in fact the transformation (59) is simply a stereographic projection of the Poincaré sphere onto the complex plane.

### 3.5 Symmetries and Other Properties of the Characteristic Waves

There are several properties of the characteristic waves that should be mentioned either because they help us understand results or because they are useful in simplifying engineering calculations. We shall simply list them here, leaving their derivation as exercises.

As in Section 3.3, we begin with the tensor operator $\mathbf{N}^e$. We suppose it has eigenvalues, $\rho_1$, $\rho_2$, and corresponding eigenvectors, $\mathbf{v}_1$, $\mathbf{v}_2$.

*Property 1.* The eigenvalues $\rho_1$, $\rho_2$ have positive imaginary parts, thus ensuring that the characteristic waves are attenuated with distance. This follows from the fact that the $N_\alpha$ have positive imaginary parts and that the $\mathbf{Q}_\alpha^m$ of (35) are positive semidefinite Hermitian symmetric matrices.

*Property 2.* The two eigenvectors satisfy

$$v_{1x}v_{2x} - v_{1y}v_{2y} = 0 \tag{61}$$

This is an analog to the orthogonal relation satisfied by eigenvectors of a symmetric matrix. It comes about because the two off-diagonal elements of $\mathbf{N}^e$ are negatives of each other.

*Property 3.* A corollary to Property 2 is that if $\mathbf{v} = (v_x, v_y)$ is an eigenvector, then the second eigenvector can be represented by $(v_y, v_x)$.

*Property 4.* A corollary to Property 3 is that if an eigenvector has normalized Stokes parameters $(g_1, g_2, g_3)$ then the second eigenvector has the normalized Stokes parameters $(-g_1, g_2, -g_3)$. Thus $g_2$ remains fixed while the other two parameters change sign. The two eigenvectors are orthogonal if and only if $g_2 = 0$.

*Property 5.* Recall that $\phi$ is the angle between the geomagnetic field and the direction of propagation. Let us replace it by $\phi' = \pi - \phi$ and then consider the resultant eigenvalues $\rho'$ and eigenvectors $\mathbf{v}'$. Since the sine of this angle remains the same while the cosine changes sign, the effect on $\mathbf{N}^e$ will be only to change the signs of the two off-diagonal elements. Thus the trace and determinant are unchanged so $\rho_j' = \rho_j$ and

$$\mathbf{v}_j' = (-v_{jx}, v_{jy}) \ . \tag{62}$$

If $(g_1, g_2, g_3)$ are the normalized Stokes parameters for one of the original eigenvectors, then $(g_1, -g_2, -g_3)$ are normalized Stokes parameters for the corresponding new eigenvector.

*Property 6.* A corollary to Property 5 is that propagation in this medium does not satisfy the laws of reciprocity. If we reverse the direction of propagation, we change the angle $\phi$ to $\pi - \phi$, and although the eigenvalues remain unchanged, the eigenvectors do not. An initial field vector is resolved into different components, thus leading to different results.

Actually, we must be cautious in making these statements because another effect here is to change the coordinate system. In reversing the direction of propagation, we have replaced $\mathbf{e}_z$ by $\mathbf{e}_z' = -\mathbf{e}_z$. It will then follow that $\mathbf{e}_x' = -\mathbf{e}_x$ and $\mathbf{e}_y' = \mathbf{e}_y$, and that therefore (62) may be written $\mathbf{v}_j' = \mathbf{v}_j$. As vectors showing magnitude and direction in three-dimensional space, the eigenvectors are also unchanged.

Nevertheless, because the direction of propagation is an important part of the definition of polarization, our original statements are still valid. Consider, for example, two right-handed helical antennas pointed at each other along a line parallel to the geomagnetic field. In the direction of the field, radio waves are attenuated at a rate proportional to $Im[N_+]$. In the opposite direction, the rate of attenuation is proportional to $Im[N_-]$.

*Property 7.* Let $\Delta f$ be the deviation of the frequency from the unsplit line center frequency; in the notation of Section 2,

$$\Delta f = f - \nu_o \ . \tag{63}$$

The refractivities $N_\alpha$ and all consequent objects may then be treated as functions of $\Delta f$. From (12) and Table 3, it may be shown that

$$N_o(-\Delta f) = -N_o(\Delta f)^*, \quad N_+(-\Delta f) = -N_-(\Delta f)^*, \quad N_-(-\Delta f) = -N_+(\Delta f)^*. \tag{64}$$

Let $\rho_j$ be the eigenvalues and $\mathbf{v}_j$ the corresponding eigenvectors when the frequency deviation has the value $\Delta f$, and consider the case when the frequency deviation equals $-\Delta f$. It will turn out that now $-\rho_j^*$ are the eigenvalues and that $v_j^*$ are the corresponding eigenvectors.

Note that we cannot state an equality between particular eigenvalues but only between sets of the two eigenvalues. For example, consider the case when $\Delta f = 0$. Then we cannot say $\rho_1 = -\rho_1^*$. We can only say that either this is true or that $\rho_1 = -\rho_2^*$.

*Property 8.* To find simpler formulas for the eigenvalues and eigenvectors, we write

$$\mathbf{N}^e = (N_+ + N_-)\mathbf{I} + (N_+ - N_-)\mathbf{S}, \tag{65}$$

where

$$\mathbf{S} = \begin{bmatrix} 2s\sin^2\phi & -i\cos\phi \\ i\cos\phi & 0 \end{bmatrix} \tag{66}$$

and

$$s = \frac{N_o - N_+ - N_-}{2(N_+ - N_-)} \ .$$

Let $\sigma_1$, $\sigma_2$ be the two eigenvalues of $\mathbf{S}$ and let $\mathbf{v}_1$, $\mathbf{v}_2$ be the corresponding eigenvectors. Then the $\mathbf{v}_j$ are also eigenvectors of $\mathbf{N}^e$ and they correspond to the eigenvalues

$$\rho_j = (N_+ + N_-) + (N_+ - N_-)\sigma_j. \tag{67}$$

We have

$$\sigma_1\sigma_2 = \det(\mathbf{S}) = -\cos^2\phi \tag{68}$$
$$\sigma_1+\sigma_2 = \text{trace}(\mathbf{S}) = 2s\sin^2\phi$$

and, for example,

$$\mathbf{v}_j = \begin{bmatrix} \sigma_j \\ i\cos\phi \end{bmatrix} \tag{69}$$

Of course, it is still true that $\mathbf{v}_2$ can be obtained by interchanging the components of $\mathbf{v}_1$.

*Property 9.* Until now we have implied that there are always two different, linearly independent eigenvectors so that, for example, (47) always has a solution. As it turns out, this is not true. To see how this might happen, we first look for conditions when the eigenvalues are equal.

The discriminant involved in solving (68) for the eigenvalues of S has the form

$$(\sigma_1-\sigma_2)^2/4 = s^2\sin^4\phi + \cos^2\phi \tag{70}$$

and this vanishes if

$$\frac{\cos\phi}{\sin^2\phi} = \pm is. \tag{71}$$

The left side here is real and so a solution can exist only if s is pure imaginary. Let us assume this condition is satisfied and then let $\phi_o$ be the unique solution to (71) for which $0 < \phi_o < \pi/2$. The solution with the opposite sign will have the angle $\pi - \phi_o$. For the first solution, the resultant single eigenvalue is

$$\sigma = s\sin^2\phi_o = \pm i\cos\phi_o \tag{72}$$

and there is only one eigenvector,

$$\mathbf{v} = \begin{bmatrix} \pm 1 \\ 1 \end{bmatrix} \tag{73}$$

where in both equations, the ambiguous sign equals the sign of the imaginary part of s. Note that the eigenvector is linearly polarized and is tilted 45° to both the x- and y-axes.

We are still left with the question of whether s can be pure imaginary. The quantity s as defined in (66) is a function of pressure, temperature, and particularly of the frequency deviation $\Delta f$. It would then not seem surprising to find that

$$Re[s(\Delta f)] = 0 \tag{74}$$

has one or more solutions. Indeed, from (64) there follows

$$s(-\Delta f) = -s(\Delta f)^* \tag{75}$$

so that $\Delta f = 0$ is always one such solution. As it turns out, however, there are (depending on pressure, temperature, and line number) quite likely to be additional solutions.

To summarize, we first solve (74) for frequency deviations $\Delta f$ and then (71) for particular angles $\phi_o$. For such special pairs of frequency and propagation direction, the problem of characteristic waves becomes degenerate. We can still evaluate the exponential in (40) but the process must be somewhat different.

*Property 10.* Let us consider the eigenvalues and eigenvectors as functions of the angle $\phi$, all other parameters being held constant. When $\phi = 0$, the two eigenvalues of **S** are $\sigma = \pm 1$. For small $\phi$ we can expand these functions in powers of $\sin\phi$ and we find

$$\begin{aligned} \sigma_1 &= 1 + (s-1/2)\sin^2\phi + \ldots \\ \sigma_2 &= -1 + (s+1/2)\sin^2\phi + \ldots \end{aligned} \tag{76}$$

Corresponding eigenvectors are given by (69) and the normalized Stokes parameters of, say, $v_1$ are

$$\begin{aligned} g_1 + ig_2 &= s\,\sin^2\phi + \ldots \\ g_3 &= 1 - (1/2)|s|^2\sin^4\phi + \ldots \,. \end{aligned} \tag{77}$$

## 4. FEATURES OF THE PROGRAM "ZEEMAN"

The computer program ZEEMAN has been devised to perform the many calculations we have suggested and to present the results in both tabular and graphical formats. Calculations include (1) the environmental parameters of pressure, temperature, and geomagnetic field components; (2) the refractivities $N_o$, $N_+$, $N_-$; (3) the eigenvalues and eigenvectors of the refractivity tensor; (4) the combination of characteristic waves that produces a given initial polarization and how this combination changes with distance; and (5) the changes in all these quantities as a wave propagates over large distances in Earth's atmosphere. The program has been written for personal microcomputers and uses Microsoft FORTRAN and the HALO graphics package.

The program's design assumes that the problems to be treated are real world problems, and this approach extends even to the environmental parameters. Part of the required input consists of the coordinates of a location--its latitude, longitude, and altitude. Using the U. S. Standard Atmosphere (COESA, 1976) the program picks out a pressure and temperature for that altitude, and using the International Geomagnetic Reference Field (IGRF) for 1985 (Baraclough, 1985) it computes a geomagnetic field vector. The U. S. Standard Atmosphere was illustrated in Table 2 and the IGRF is displayed in Figure 6. The ellipticity of Earth must also be considered, and in this respect it is assumed that the given latitude and longitude are geodetic coordinates and that the altitude is above the local sea level. These are changed to geocentric coordinates for most of the calculations--but note that the Standard Atmosphere is always determined from the local altitude.

The program is menu driven with a question and answer segment that is meant to be self-explanatory. The first task facing a user is to define a "case" for study. This will describe the overall problem that is to be treated and will require such input parameters as altitude, latitude, and longitude; the spectral line of interest and the deviation from its central frequency; the direction of propagation (azimuth and elevation angle); and the initial polarization of the signal. If desired, after a case has been defined it may be stored in a separate disk file and retrieved at a later time.

Figure 7 shows how the program introduces itself and how the first few screens appear. Answering "P" to the last question here will cause the

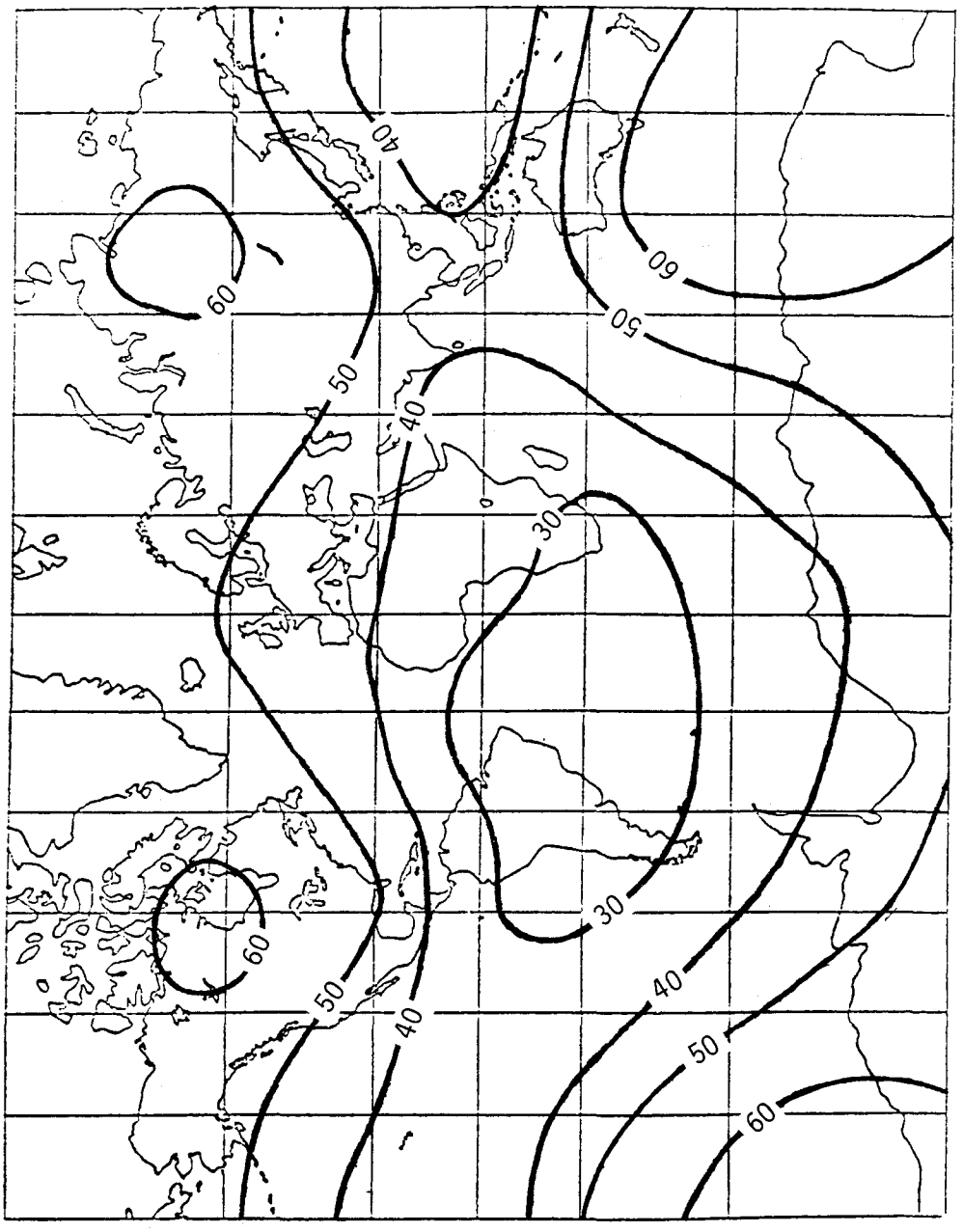


Figure 6. Magnitude of the magnetic flux density as given by the International Geomagnetic Reference Field of 1985.

```
**------------------------------------------------------------------------**
:                                                                        :
:                                                                        :
:                                                                        :
:                                                                        :
:                 Zeeman Mesosphere Wave Propagation Model V3.5           :
:                                                                        :
:                                                                        :
:                                                                        :
**------------------------------------------------------------------------**

Would you like to enter a case file? (y/n) (N)

 1) K   =     5+          FQO = 59.590980 GHz
 2) h   =   80. km     3) LAT =    .0 deg        4) LON=     .0 deg
 5) DFQ =   1.0 MHz    6) RES =  .003 MHz
 7) AZI =    .0 deg    8) ELV =    .0 deg
 9) STEP=  1000       10) INCR=   1.0 km/step
11) POL =    .0 deg   12) HZE =   .00           13) VTE =   .00
14) A   =   8.0 dB max path loss                15) Screen (X/Y)=1.00

Enter new parameters or edit individual values? (p/e) (E)
Which value to edit? ()
 1) K   =     5+          FQO = 59.590980 GHz
 2) h   =   80. km     3) LAT =    .0 deg        4) LON=     .0 deg
 5) DFQ =   1.0 MHz    6) RES =  .003 MHz
 7) AZI =    .0 deg    8) ELV =    .0 deg
 9) STEP=  1000       10) INCR=   1.0 km/step
11) POL =    .0 deg   12) HZE =   .00           13) VTE =   .00
14) A   =   8.0 dB max path loss                15) Screen (X/Y)=1.00

Are you satisfied with these values?  (y/n) (Y)
**------------------------------------------------------------------------**

What output would you prefer?
   T : tables
   G : graphs to screen (default)
   S : save parameters
(T)
Would you like output to a printer?
    0 : screen only (default)
    1 : HP LaserJet
    2 : Epson dot matrix
    3 : HP Plotter file
(2)
What would you prefer to see?
   P : Parameters of propagation case
   N : N components
   E : Eigenvalues (v1,v2)
   C : Characteristic waves
   S : Radio wave propagation (Stokes' parameters, polarization, attn.)
```

Figure 7. The first few screens displayed by program ZEEMAN.

program to display a neatly written summary of the parameters of the case under current consideration. In Figure 8 we have printed out this summary for the Default Case that is coded into the program.

### 4.1. N Components

Answering "N" to the last question of Figure 7 will produce displays of first the real parts and second the imaginary parts of the three components $N_o$, $N_+$, $N_-$. They are shown as functions of the frequency deviation $\Delta f$ and are computed from the formulas of Section 2.2. Normally the computations involve one single $K^{\pm}$ line, but for the four doublets flagged in Table 1, requests for one of the lines will always bring in the other as well.

In Figure 9 the graphical output is shown for the Default Case of Figure 8. In Figure 10 the corresponding tabular results are shown, where, however, we have changed RES, the frequency resolution, to 0.05 MHz so as to allow the results to appear on a single page.

### 4.2. Eigenvalues

If "E" is the answer to the last question in Figure 7, the program will compute and display the two eigenvalues of the matrix $\mathbf{N}^e$. These will be treated as functions of either the angle $\phi$ or the frequency deviation $\Delta f$. For the Default Case we show in Figure 11 the real and imaginary parts of the eigenvalues versus the angle $\phi$ and in Figure 12 versus the frequency deviation. In Figure 13 we again show the eigenvalues plotted against $\phi$ but now with $\Delta f = 0$; and the warnings of Section 3.5 become more concrete. When $\phi$ is near 0° or 180°, the two imaginary parts are equal and with $\phi$ near 90°, the real parts are equal. At about 66.1° and 113.9° both parts are equal and the refractivity matrix becomes degenerate.

### 4.3. Characteristic Waves

If "C" is the answer to the last question in Figure 7, the resultant responses concern the characteristic waves. These are represented by the normalized Stokes parameters, $g_1$, $g_2$, $g_3$, and are plotted as functions of the angle $\phi$ in two different ways.

```
                              SUMMARY
     Mesospheric Propagation near an Oxygen Microwave Line (Zeeman Effect)
**-------------------------------------------------------------------------**
          INPUT:          |
                          |      1. GEODETIC COORDINATES
                          |
    h    =     80 km      | (30-100 km, U.S. Std. Atmosphere 1976)
    LAT  =      .0 deg    | (0 = equator, 90 = north pole, -90 = south pole)
    LON  =      .0 deg    | (0 = Greenwich, +180 East, -180 West)
                          |
                          |      2. GEOMAGNETIC FIELD
                          |
                          |  East = -4.3006 uT  (microTesla)
                          |  North= 26.5012 uT
                          |  Up   = 13.0993 uT
                          | |B|   = 29.8731 uT     Dip Angle= -26.0 deg
                          |
                          |      3. OXYGEN SPECTRAL LINE
                          |
    K    =      5+        | (42 lines)   FQ0= 59590.980 MHz
                          |
                          |      4. RADIOWAVE CHARACTERIZATION
                          |
                          |a) Frequency:
    DFQ  =   1.00 MHz     | (MAX. +/- 250 MHz)
                          |
                          | FQ = FQ0 + DFQ  =   59591.980 MHz
                          |
    RES  =   .003 MHz     | (MAX. 2000 points = 2*DEV/RES + 1)
                          |
                          |b) Direction:
    AZI  =      .0 deg    | (0 = N, 90 = E, 180 = S, 270 = W)
    ELV  =      .0 deg    | (0 = Horizontal, 90 = Vertical)
                          |
                          | Phi =   27.5 deg  ( 0 = parallel to |B|,
                          |                     90 = perpend. to |B|)
                          |
                          |c) Initial Polarization:
    HZE  =      .0        | HZE = 0 or VTE = 0 --> linear polariz. (e.g. HL,VL)
    VTE  =      .0        | HZE = VTE, POL = 90 --> RightCircular (-90 = LeftC)
    POL  =      .0 deg    | Phase angle or linear polariz. orient. angle (0 = HL)
                          |
                          |d) Path Length:
    STEP=    1000         | (10 intervals are marked)
    INCR=     1.0 km/step |
                          |
                          |e) Max. Attenuation Tolerated by Path:
    A    =       8 dB     |
**-------------------------------------------------------------------------**
```

Figure 8. The "Summary of Parameters" for the "Default Case" for program ZEEMAN.

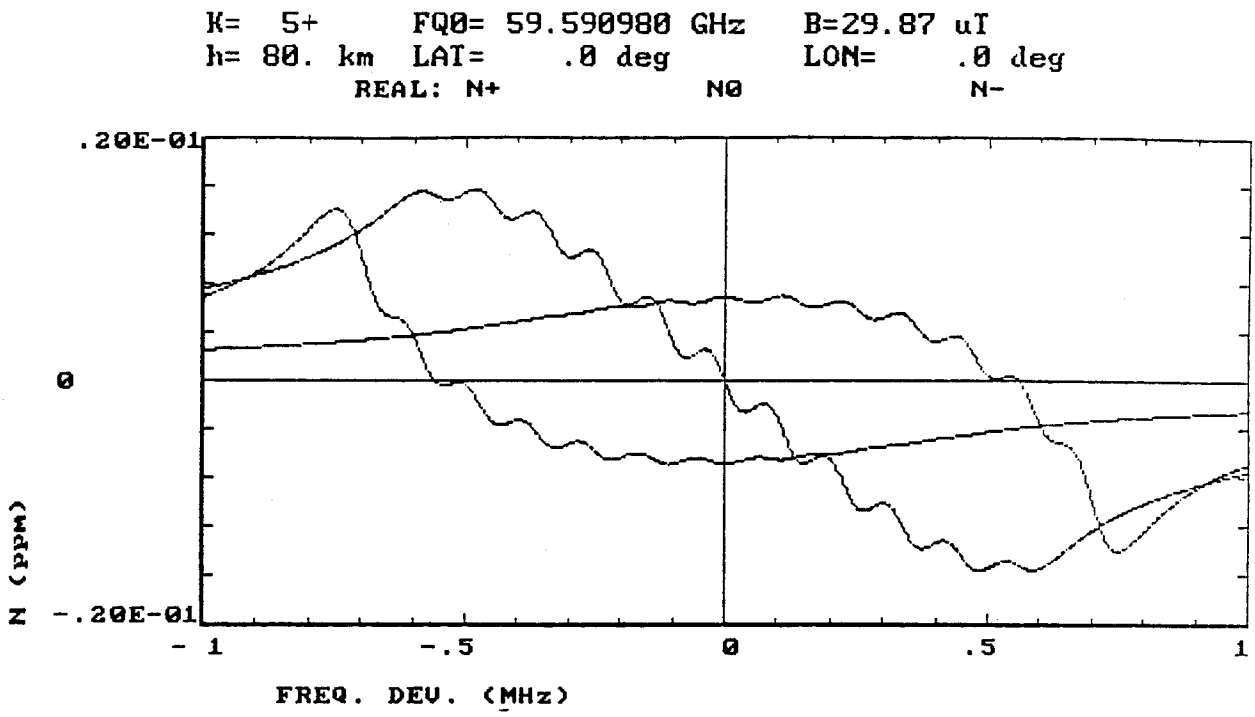


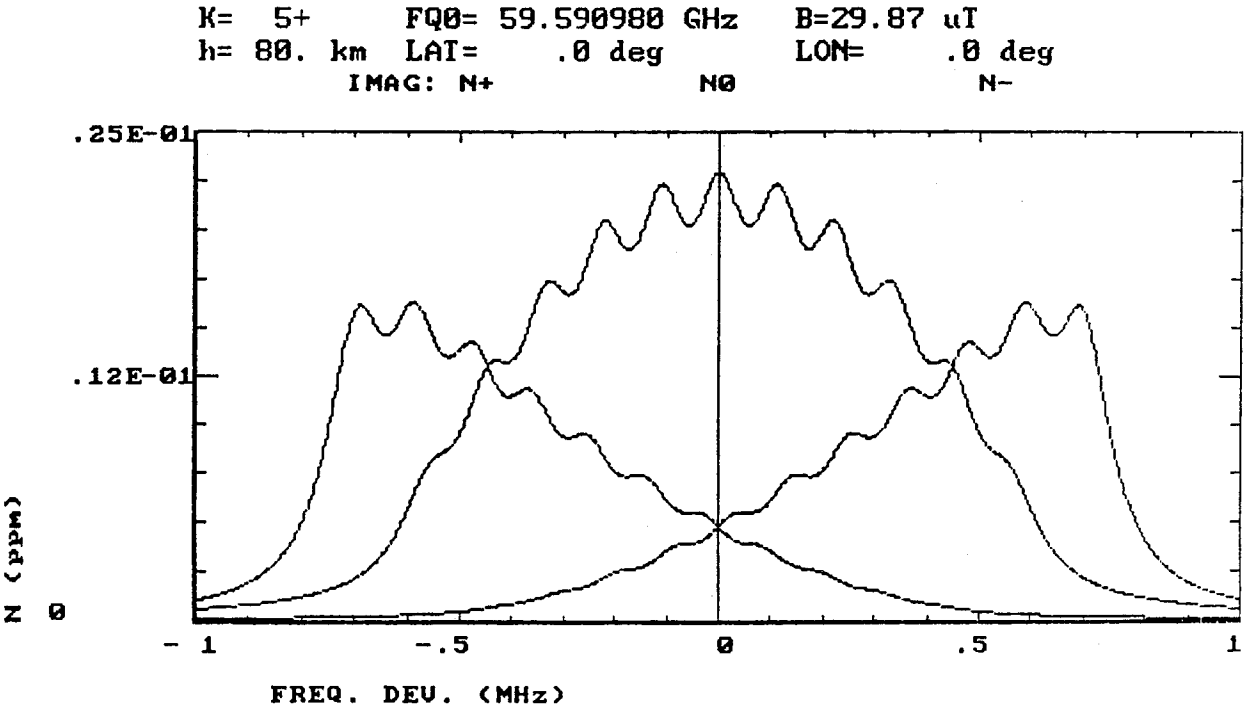


Figure 9. Real and imaginary parts of the N components for the Default Case.

K= 5+ FQO= 59.590980 GHz B=29.87 uT
h= 80. km LAT= .0 deg LON= .0 deg

| FREQ. DEV (MHz) | CNO (ppm) Re | CNO (ppm) Im | CN+ (ppm) Re | CN+ (ppm) Im | CN- (ppm) Re | CN- (ppm) Im |
|---|---|---|---|---|---|---|
| -1.000 | .758E-02 | .609E-03 | .690E-02 | .106E-02 | .253E-02 | .127E-03 |
| -.950 | .808E-02 | .704E-03 | .777E-02 | .140E-02 | .263E-02 | .138E-03 |
| -.900 | .865E-02 | .828E-03 | .891E-02 | .195E-02 | .274E-02 | .151E-03 |
| -.850 | .933E-02 | .994E-03 | .104E-01 | .294E-02 | .286E-02 | .166E-03 |
| -.800 | .101E-01 | .123E-02 | .124E-01 | .498E-02 | .299E-02 | .184E-03 |
| -.750 | .111E-01 | .158E-02 | .141E-01 | .961E-02 | .314E-02 | .206E-03 |
| -.700 | .124E-01 | .216E-02 | .100E-01 | .159E-01 | .331E-02 | .233E-03 |
| -.650 | .140E-01 | .327E-02 | .530E-02 | .147E-01 | .350E-02 | .268E-03 |
| -.600 | .155E-01 | .557E-02 | .366E-02 | .161E-01 | .372E-02 | .313E-03 |
| -.550 | .150E-01 | .818E-02 | -.312E-03 | .144E-01 | .397E-02 | .379E-03 |
| -.500 | .155E-01 | .957E-02 | -.410E-03 | .139E-01 | .427E-02 | .485E-03 |
| -.450 | .146E-01 | .130E-01 | -.342E-02 | .132E-01 | .458E-02 | .672E-03 |
| -.400 | .134E-01 | .133E-01 | -.325E-02 | .115E-01 | .486E-02 | .878E-03 |
| -.350 | .131E-01 | .166E-01 | -.503E-02 | .114E-01 | .523E-02 | .115E-02 |
| -.300 | .101E-01 | .168E-01 | -.522E-02 | .937E-02 | .545E-02 | .154E-02 |
| -.250 | .106E-01 | .188E-01 | -.582E-02 | .945E-02 | .582E-02 | .183E-02 |
| -.200 | .653E-02 | .199E-01 | -.641E-02 | .761E-02 | .603E-02 | .246E-02 |
| -.150 | .690E-02 | .199E-01 | -.620E-02 | .740E-02 | .623E-02 | .273E-02 |
| -.100 | .312E-02 | .221E-01 | -.693E-02 | .612E-02 | .656E-02 | .357E-02 |
| -.050 | .240E-02 | .203E-01 | -.640E-02 | .551E-02 | .642E-02 | .395E-02 |
| .000 | -.183E-07 | .230E-01 | -.692E-02 | .479E-02 | .692E-02 | .479E-02 |
| .050 | -.240E-02 | .203E-01 | -.642E-02 | .395E-02 | .640E-02 | .551E-02 |
| .100 | -.312E-02 | .221E-01 | -.656E-02 | .357E-02 | .693E-02 | .612E-02 |
| .150 | -.690E-02 | .199E-01 | -.623E-02 | .273E-02 | .620E-02 | .740E-02 |
| .200 | -.653E-02 | .199E-01 | -.603E-02 | .246E-02 | .641E-02 | .761E-02 |
| .250 | -.106E-01 | .188E-01 | -.582E-02 | .183E-02 | .582E-02 | .945E-02 |
| .300 | -.101E-01 | .168E-01 | -.545E-02 | .154E-02 | .522E-02 | .937E-02 |
| .350 | -.131E-01 | .166E-01 | -.523E-02 | .115E-02 | .503E-02 | .114E-01 |
| .400 | -.134E-01 | .133E-01 | -.486E-02 | .878E-03 | .325E-02 | .115E-01 |
| .450 | -.146E-01 | .130E-01 | -.458E-02 | .672E-03 | .342E-02 | .132E-01 |
| .500 | -.155E-01 | .957E-02 | -.427E-02 | .485E-03 | .410E-03 | .139E-01 |
| .550 | -.150E-01 | .818E-02 | -.397E-02 | .379E-03 | .312E-03 | .144E-01 |
| .600 | -.155E-01 | .557E-02 | -.372E-02 | .313E-03 | -.366E-02 | .161E-01 |
| .650 | -.140E-01 | .327E-02 | -.350E-02 | .268E-03 | -.530E-02 | .147E-01 |
| .700 | -.124E-01 | .216E-02 | -.331E-02 | .233E-03 | -.100E-01 | .159E-01 |
| .750 | -.111E-01 | .158E-02 | -.314E-02 | .206E-03 | -.141E-01 | .961E-02 |
| .800 | -.101E-01 | .123E-02 | -.299E-02 | .184E-03 | -.124E-01 | .498E-02 |
| .850 | -.933E-02 | .994E-03 | -.286E-02 | .166E-03 | -.104E-01 | .294E-02 |
| .900 | -.865E-02 | .828E-03 | -.274E-02 | .151E-03 | -.891E-02 | .195E-02 |
| .950 | -.808E-02 | .704E-03 | -.263E-02 | .138E-03 | -.777E-02 | .140E-02 |
| 1.000 | -.758E-02 | .609E-03 | -.253E-02 | .127E-03 | -.690E-02 | .106E-02 |

Figure 10. The tabular display of the N components for the Default Case.

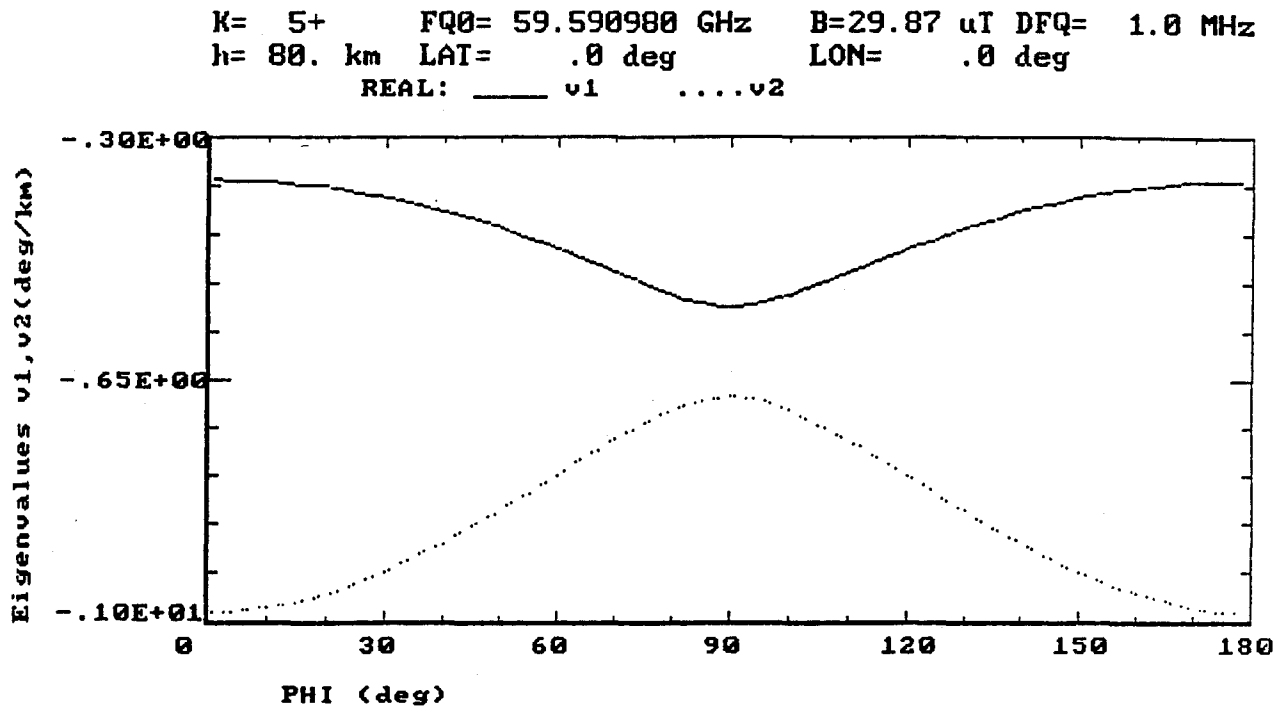


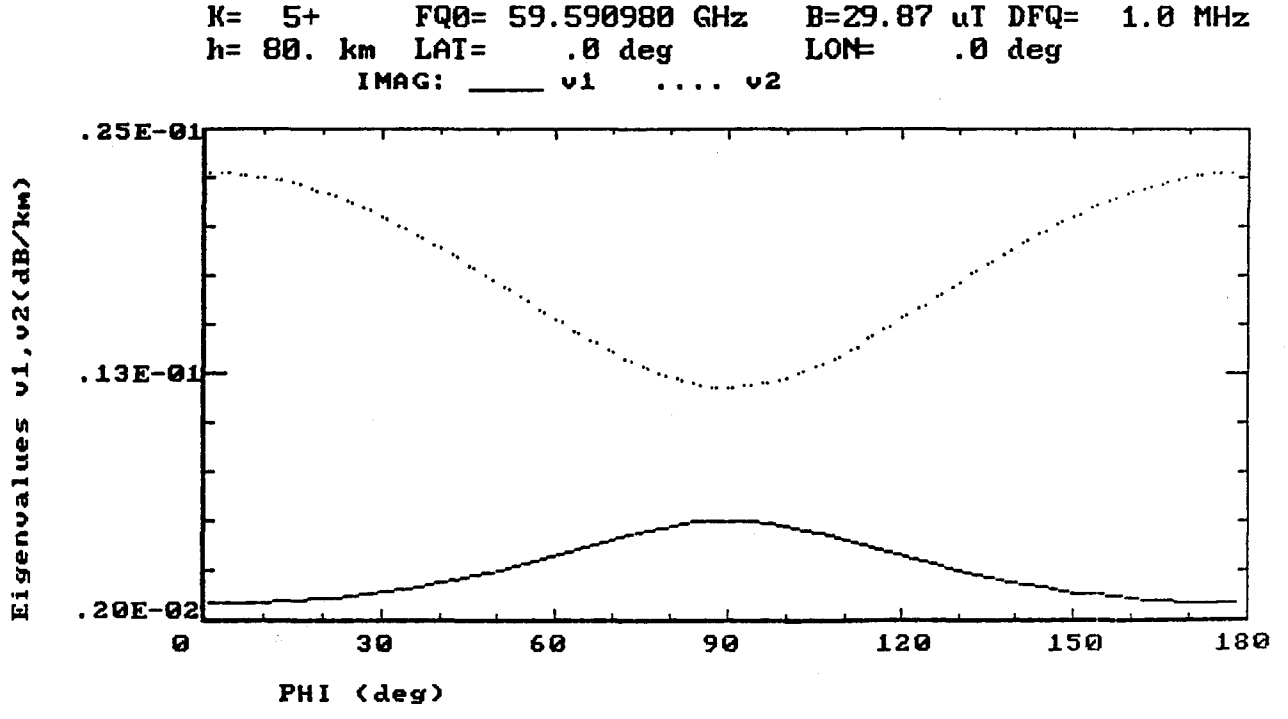


Figure 11. The eigenvalues for the Default Case. Real parts and imaginary parts plotted against the angle $\phi$.

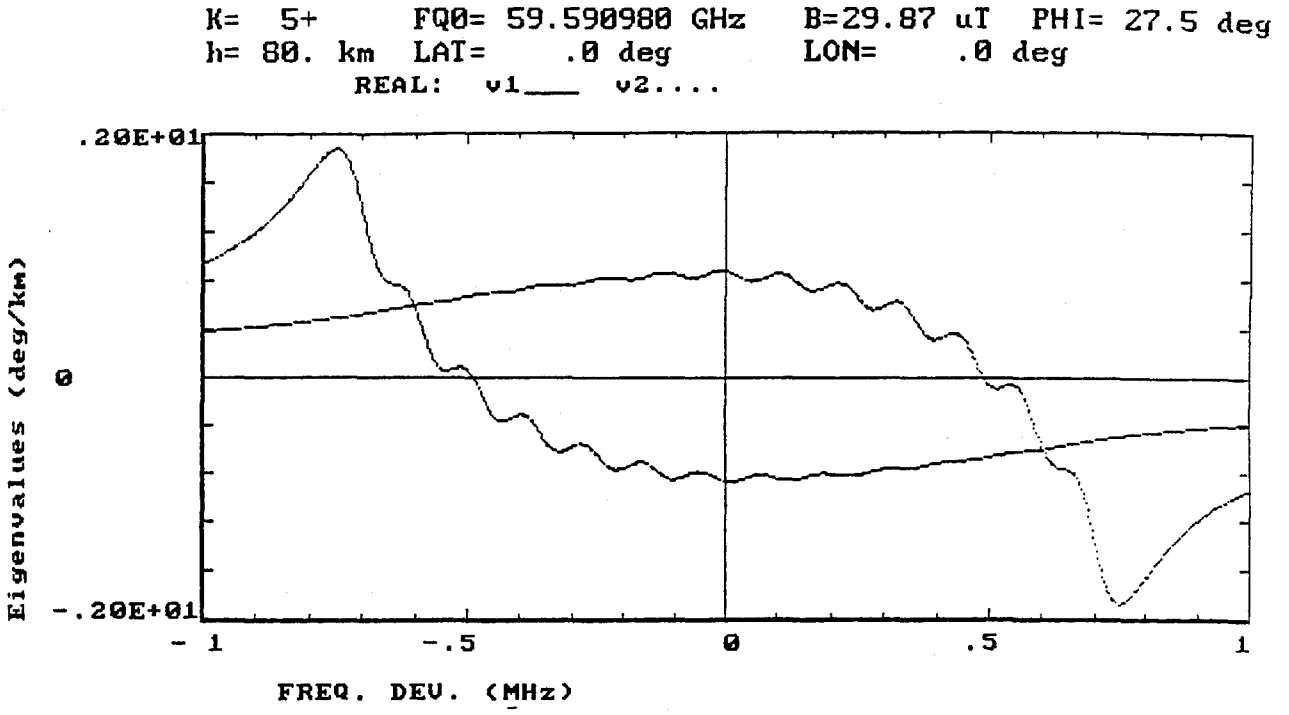


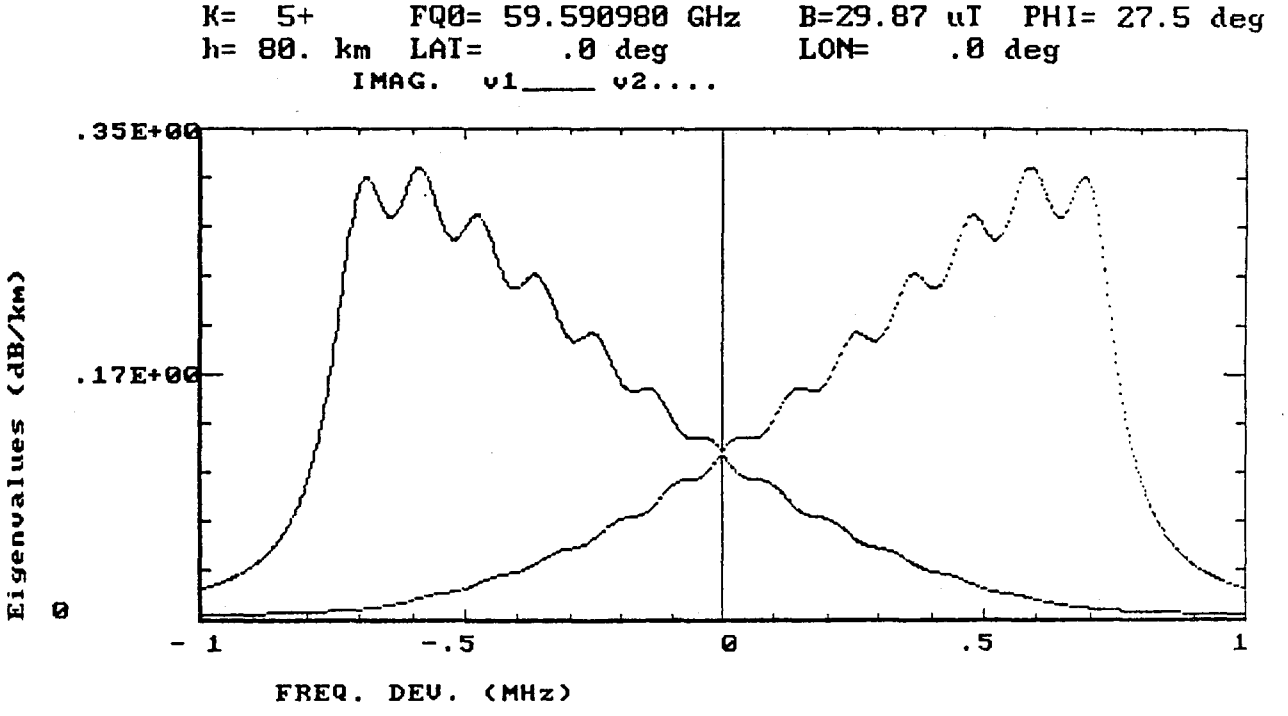


Figure 12. The eigenvalues for the Default Case. Real parts and imaginary parts plotted against the frequency deviation $\Delta f$

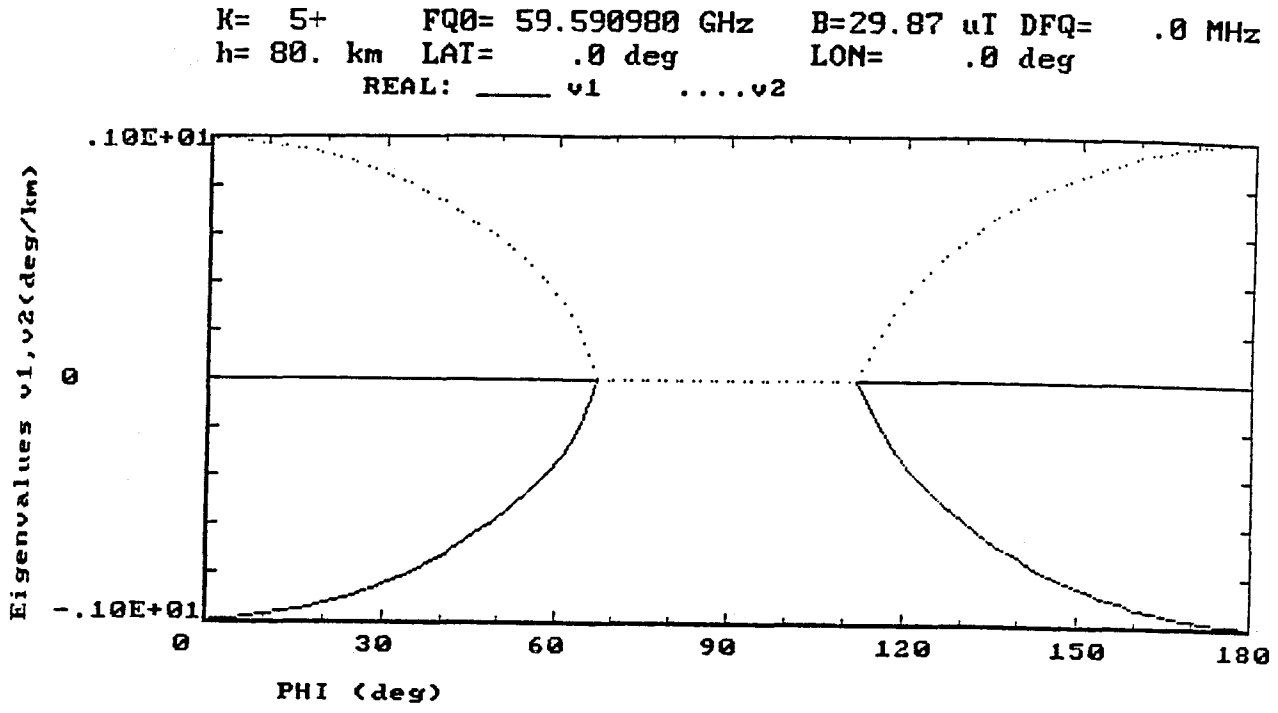


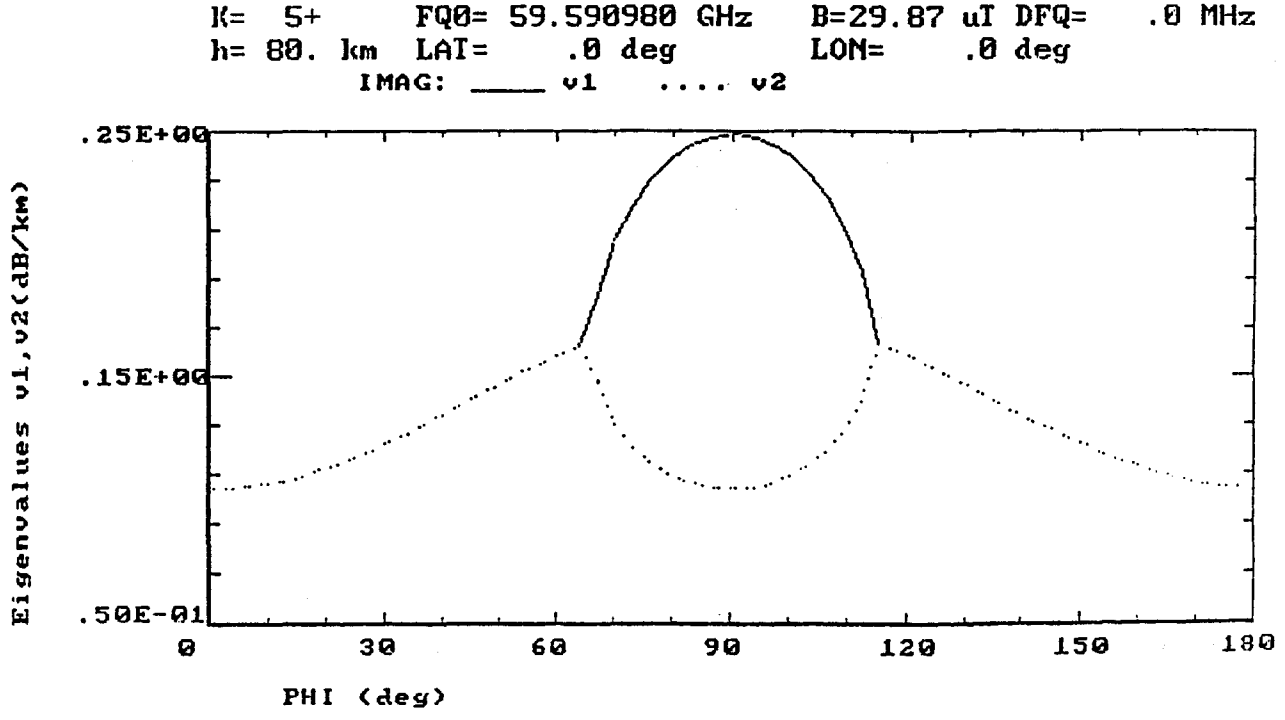


Figure 13. The eigenvalues for the Default Case where, however, $\Delta f = 0$. Real parts and imaginary parts plotted against the angle $\phi$.

The first of these ways is illustrated in Figure 14. It is a simple plot of the three functions that correspond to one of the eigenvectors. As we have seen, the Stokes parameters for the other eigenvector are the same except that $g_1$ and $g_3$ have opposite signs.

In the second plot the Poincaré sphere is pictured and the eigenvectors are represented by their trajectories on the sphere using $\phi$ as the parameter. To better read these graphs one should remember that the eigenvectors are circularly polarized (at the North and South Poles) when $\phi$ is 0° or 180° and linearly polarized (on the Equator) when $\phi$ is 90°. The results for the Default Case are shown in Figure 15. Note that the display shows two orthographic projections. On the left is an oblique projection with the $g_3$ axis vertical. On the right is a polar projection in which the vantage point is directly above the sphere.

### 4.4. Radio Wave Propagation

The actual properties of a propagating wave with an initial arbitrary polarization are provided when "S" is given in answer to the question in Figure 7. There are four graphical options. The first three of these are concerned with propagation through a homogeneous medium having the properties of the atmosphere at the selected location. This notion is not very realistic if the path is more than a few hundred kilometers long.

In the first option there is plotted the trajectory of the electric field on the normalized Poincaré sphere. These are portrayed using an oblique orthographic projection as illustrated in Figure 16. Note how in that figure the trajectory, which starts with horizontal linear polarization at the Equator, spirals around the sphere and seems to tend toward some point nearly at the North Pole. Indeed, as one sees from Figure 14, the eigenvectors are nearly circularly polarized, and Figure 16 shows us that the left-hand polarized part of the original wave is the more severely attenuated so that the wave here tends asymptotically to its right-hand polarized part. Information on how the wave progresses along this trajectory is provided by some 10 "tick" marks that are inserted at equal distances. In the present case, these ticks are 100 km apart.

The second option to display radio wave propagation is illustrated in Figure 17. This is a simple plot of attenuation versus distance. Note how there appear to be two different rates of attenuation. This occurs because at

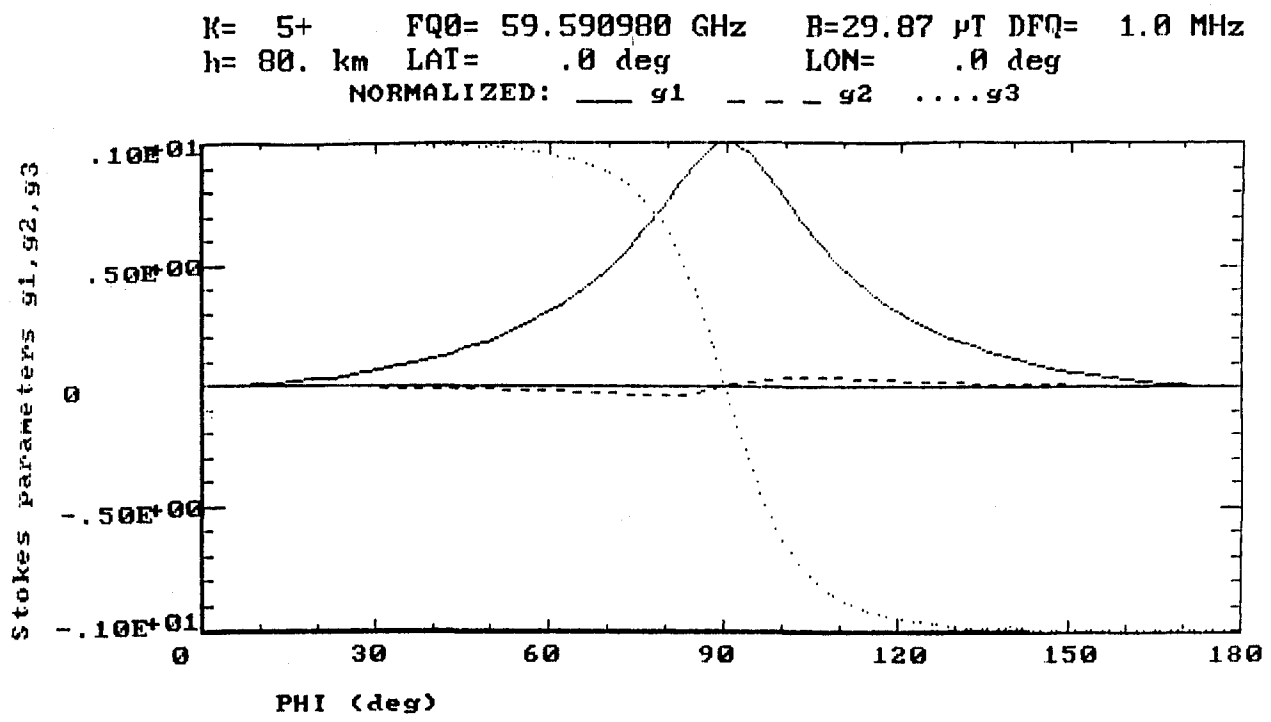


Figure 14. Normalized Stokes parameters of the eigenvectors for the Default Case plotted against the angle $\phi$.

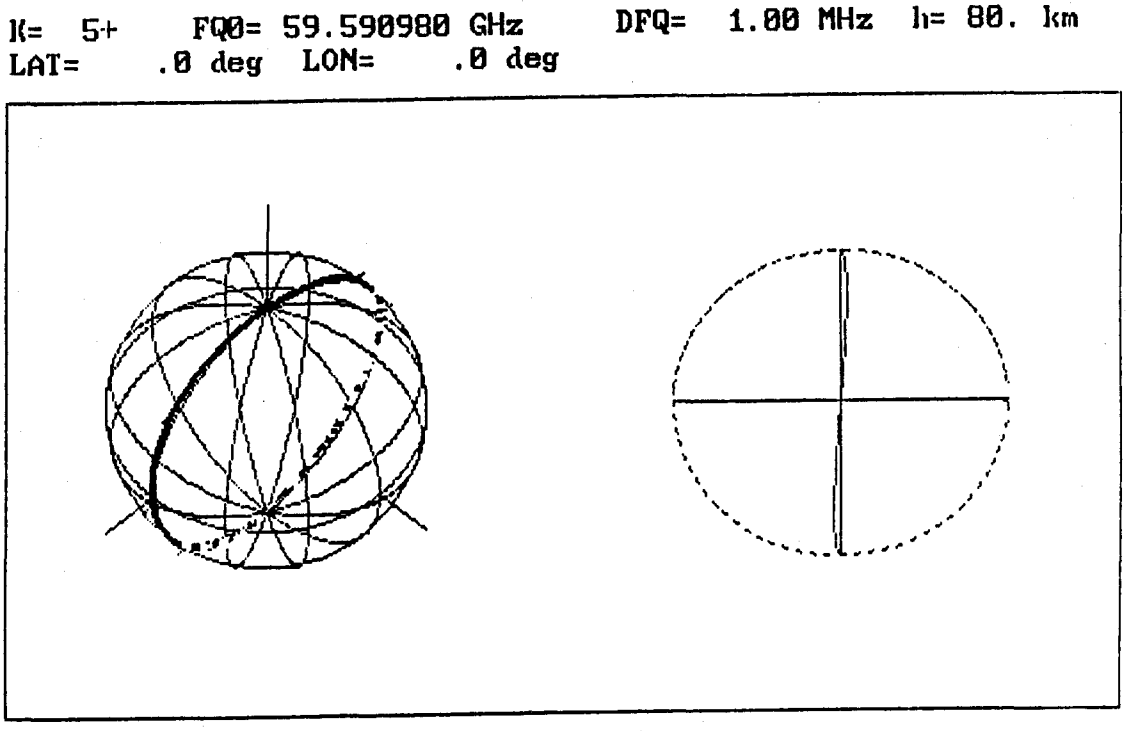


Figure 15. Trajectories of the eigenvectors for the Default Case as plotted on the Poincaré sphere.

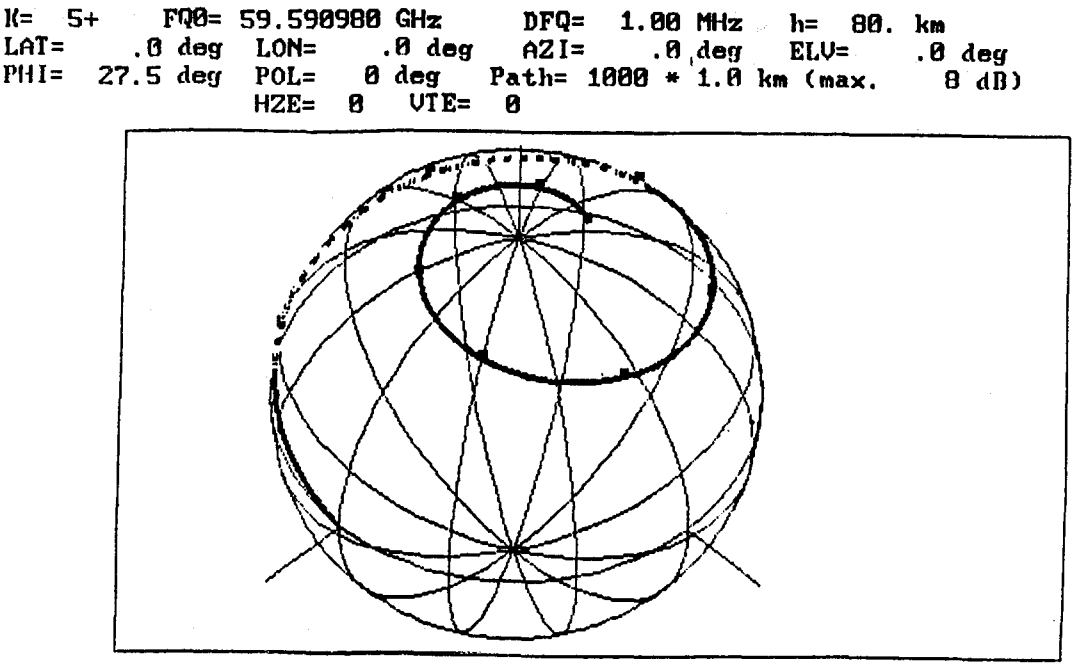


Figure 16. The trajectory on the Poincaré sphere of a wave propagating through mesospheric-like medium. Parameters are those of the Default Case.

the beginning there is a left-hand polarized part that is attenuated at a relatively high rate. When it has nearly disappeared, there is left only the right-hand polarized wave with its more sedate attenuation rate.

The third option available here provides a more pictorial representation of what happens to the polarization. At 10 equally spaced points along the path, the program stops and plots an ellipse of the proper ellipticity and orientation to imitate the trajectory in space of the electric field vector. The example in Figure 18 shows these ellipses every 100 km at just the marked points in Figure 16. Note how they steadily become more nearly circular and how they appear to rotate. The letter "-R-" that appears above each ellipse indicates that they are all traversed in the right-hand direction.

The final option here is of a somewhat different nature. The given location and the azimuth and elevation angles are all used as initial values for a wave that passes through the real-world mesosphere and emerges either at the lower boundary of 30 km or the upper at 100 km. In the course of this passage, the pressure, temperature, geomagnetic field, and the angle to the direction of propagation all change along the indicated path. The computations must find these changes and then must include them in an integration of the two-dimensional differential equation

```
K=  5+     FQ0= 59.590980 GHz     DFQ=   1.00 MHz   h=  80. km
LAT=      .0 deg   LON=      .0 deg   AZI=      .0 deg   ELV=      .0 deg
PHI=  27.5 deg   HZE=  0 VTE=  0 POL=    0 deg
```

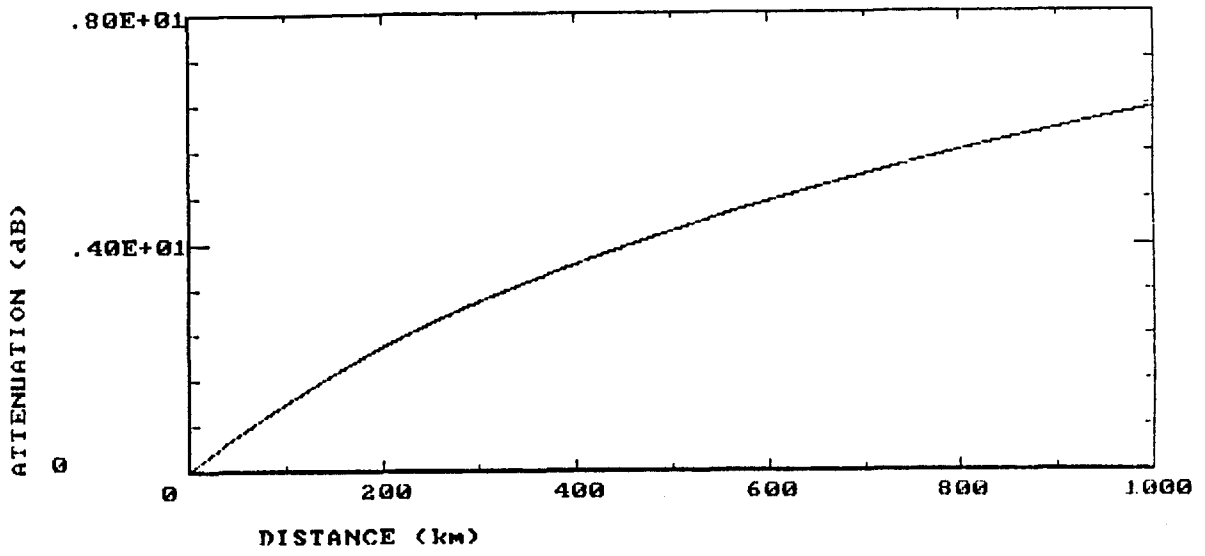


Figure 17. Attenuation versus distance for the wave in Figure 16.

```
K=  5+     FQ0= 59.590980 GHz     DFQ=   1.00 MHz   h= 80. km
LAT=      .0 deg   LON=      .0 deg   AZI=      .0 deg   ELV=      .0 deg
PHI=  27.5 deg   POL=    0 deg    Path= 1000 * 1.0 km (max.     8 dB)
                 HZE=  0   VTE=  0
```

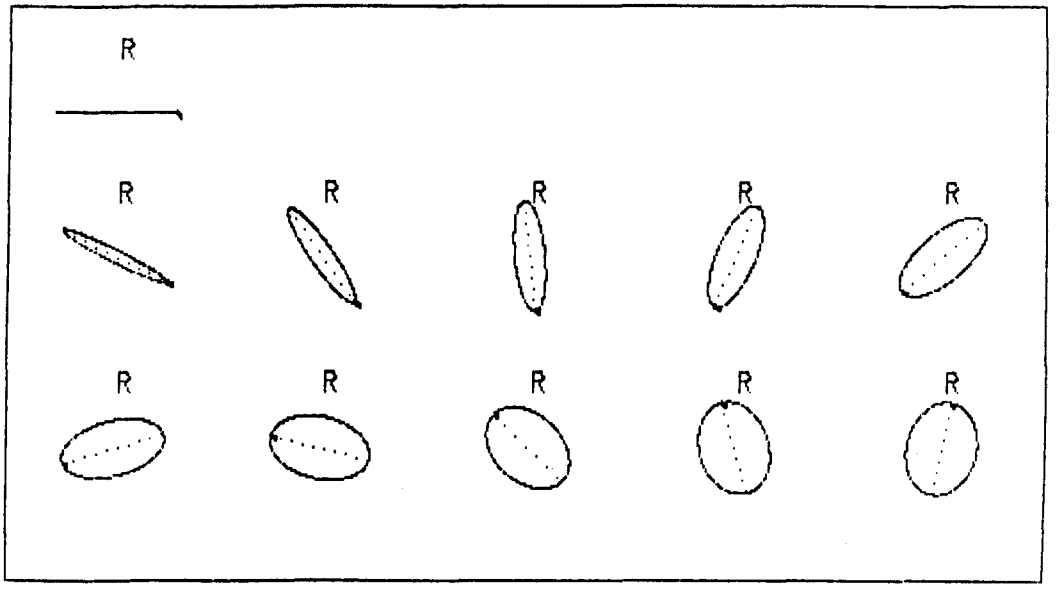


Figure 18. Elliptical trajectories of the electric field at selected distances for the wave depicted in Figure 16.

$$dE/dz = ik(\mathbf{I} + \mathbf{N}^e)E,$$

where now the matrix $\mathbf{N}^e$ is a (known) function of z. This equation is an approximation--for example, a changing refractivity implies a bending ray--but again, because $\mathbf{N}^e$ is small, the approximation is a very good one.

In actual operation the program now performs this integration three separate times using three different initial polarizations: left circular, horizontal linear, and right circular. The graphical output for the Default Case is reproduced in Figure 19. Note how the total attenuations are given in the header and how the elliptical trajectories for each of the three polarizations are depicted below.

### 4.5. Propagation through the Mesosphere

There are two further program segments or overlays that help make up the ZEEMAN whole. Both segments are used, as was the last option above, to explore how a radio wave travels through a real-world mesosphere. The path begins at the selected location and ends when it has emerged from the mesosphere at either 30 km or 100 km altitude. Input to either program segment is by means of a "case file" that has been constructed in the main program segment and saved as a separate file.

The first of these additional segments is called MPI--the "mesospheric integrator." It has no graphical output, but as illustrated in Figure 20, it produces a table showing how the wave progresses as it passes through each kilometer-thick layer. The columns give in succession the latitude, longitude, and altitude along the path, the azimuthal heading, the elevation angle, the magnitude of the magnetic flux density, the angle $\phi$, the attenuation the wave has suffered, the polarization, and the total distance that has been traveled. The polarization is defined by giving the magnitude of the horizontal component, the magnitude of the vertical component, and the phase angle by which the vertical component lags the horizontal component. This is all normalized by requiring the horizontal component to have unit size; this description is therefore almost identical with Beckmann's notation as given in Section 3.4.

The second alternative segment is called MPF--the "mesospheric frequency integrator." It provides tables or graphs of total attenuation versus the frequency deviation. As shown in Figure 21, there are four initial polariza-

```
K=  5+     FQ0= 59.590980 GHz     DFQ=   1.00 MHz   h=100. km
LAT=    4.5 deg  LON=     .0 deg  AZI=     .0 deg  ELV=    4.5 deg
H= 1.00     V=  .91     H= 1.00     V= 3.17      H= 1.00     V= 1.04
POL= -93.4  dB=    5.6 POL= 123.3  dB=    2.7  POL=  87.3  dB=     .8
```

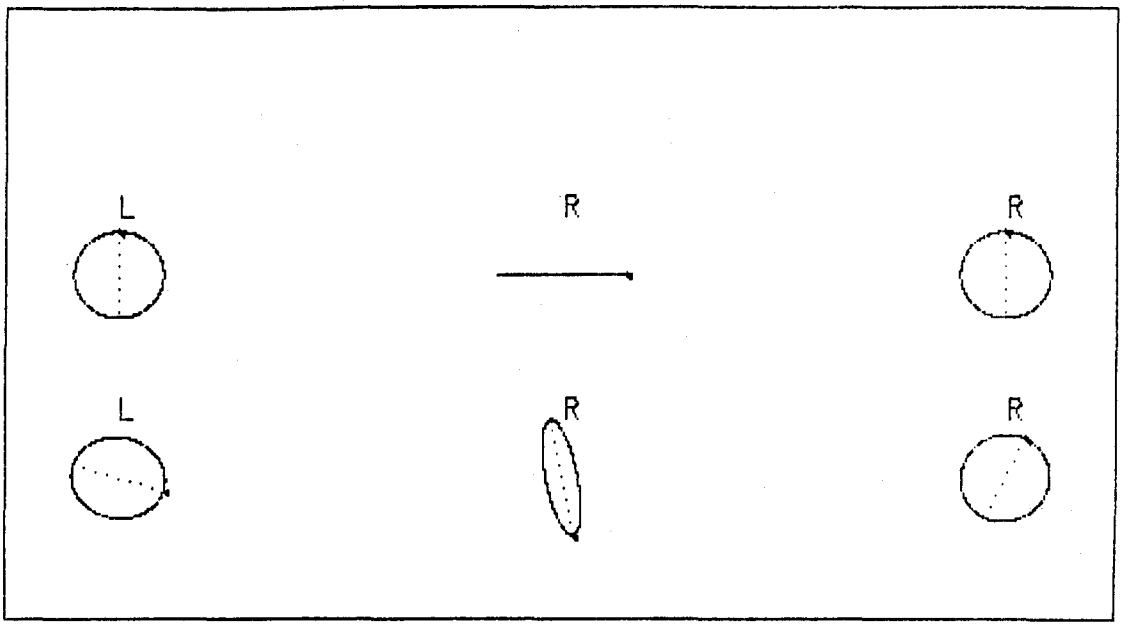


Figure 19. Total attenuation and elliptical trajectories of the electric field after a wave has emerged from the top of the mesosphere. Initial parameters are those of the Default Case and initial polarizations are left.

| LAT | LON | H | AZ | EL | \|B\| | PHI | dB | POLARIZATION | | | | S tot |
|---|---|---|---|---|---|---|---|---|---|---|---|---|
| .0 | .0 | 75 | .0 | .0 | .00 | .0 | .00 | 1.0/ | .00/ | 0 | deg | .0 |
| 1.0 | .0 | 76 | .0 | 1.0 | 29.99 | 25.9 | 2.87 | 1.0/ | 1.79/ | 143 | deg | 113.6 |
| 1.4 | .0 | 77 | .0 | 1.4 | 30.03 | 23.7 | 3.55 | 1.0/ | 2.81/ | 97 | deg | 160.7 |
| 1.8 | .0 | 78 | .0 | 1.7 | 30.05 | 22.5 | 3.92 | 1.0/ | 2.17/ | 66 | deg | 196.8 |
| 2.0 | .0 | 79 | .0 | 2.0 | 30.06 | 21.6 | 4.16 | 1.0/ | 1.61/ | 55 | deg | 227.2 |
| 2.3 | .0 | 80 | .0 | 2.3 | 30.07 | 20.7 | 4.32 | 1.0/ | 1.30/ | 53 | deg | 254.1 |
| 2.5 | .0 | 81 | .0 | 2.5 | 30.07 | 20.0 | 4.44 | 1.0/ | 1.11/ | 53 | deg | 278.3 |
| 2.7 | .0 | 82 | .0 | 2.7 | 30.07 | 19.4 | 4.53 | 1.0/ | .98/ | 54 | deg | 300.7 |
| 2.9 | .0 | 83 | .0 | 2.9 | 30.08 | 18.8 | 4.60 | 1.0/ | .90/ | 55 | deg | 321.4 |
| 3.0 | .0 | 84 | .0 | 3.0 | 30.08 | 18.2 | 4.66 | 1.0/ | .84/ | 57 | deg | 340.9 |
| 3.2 | .0 | 85 | .0 | 3.2 | 30.08 | 17.6 | 4.70 | 1.0/ | .79/ | 59 | deg | 359.4 |
| 3.4 | .0 | 86 | .0 | 3.3 | 30.08 | 17.1 | 4.73 | 1.0/ | .76/ | 61 | deg | 376.9 |
| 3.5 | .0 | 87 | .0 | 3.5 | 30.08 | 16.7 | 4.76 | 1.0/ | .74/ | 62 | deg | 393.7 |
| 3.7 | .0 | 88 | .0 | 3.6 | 30.07 | 16.2 | 4.78 | 1.0/ | .72/ | 64 | deg | 409.8 |
| 3.8 | .0 | 89 | .0 | 3.8 | 30.07 | 15.8 | 4.79 | 1.0/ | .71/ | 65 | deg | 425.3 |
| 3.9 | .0 | 90 | .0 | 3.9 | 30.07 | 15.3 | 4.81 | 1.0/ | .70/ | 66 | deg | 440.2 |
| 4.1 | .0 | 91 | .0 | 4.0 | 30.07 | 14.9 | 4.82 | 1.0/ | .69/ | 67 | deg | 454.7 |
| 4.2 | .0 | 92 | .0 | 4.2 | 30.07 | 14.5 | 4.83 | 1.0/ | .68/ | 67 | deg | 468.7 |
| 4.3 | .0 | 93 | .0 | 4.3 | 30.06 | 14.2 | 4.83 | 1.0/ | .68/ | 68 | deg | 482.3 |
| 4.4 | .0 | 94 | .0 | 4.4 | 30.06 | 13.8 | 4.84 | 1.0/ | .67/ | 68 | deg | 495.6 |
| 4.5 | .0 | 95 | .0 | 4.5 | 30.06 | 13.5 | 4.84 | 1.0/ | .67/ | 69 | deg | 508.5 |
| 4.6 | .0 | 96 | .0 | 4.6 | 30.06 | 13.1 | 4.85 | 1.0/ | .67/ | 69 | deg | 521.0 |
| 4.8 | .0 | 97 | .0 | 4.7 | 30.05 | 12.8 | 4.85 | 1.0/ | .67/ | 69 | deg | 533.3 |
| 4.9 | .0 | 98 | .0 | 4.8 | 30.05 | 12.5 | 4.85 | 1.0/ | .66/ | 69 | deg | 545.3 |
| 5.0 | .0 | 99 | .0 | 4.9 | 30.05 | 12.2 | 4.85 | 1.0/ | .66/ | 70 | deg | 557.1 |
| 5.1 | .0 | 100 | .0 | 5.0 | 30.04 | 11.9 | 4.86 | 1.0/ | .66/ | 70 | deg | 568.6 |

Figure 20. Tabular display showing how a radio wave progresses through the mesosphere. Input parameters are those of the Default Case.

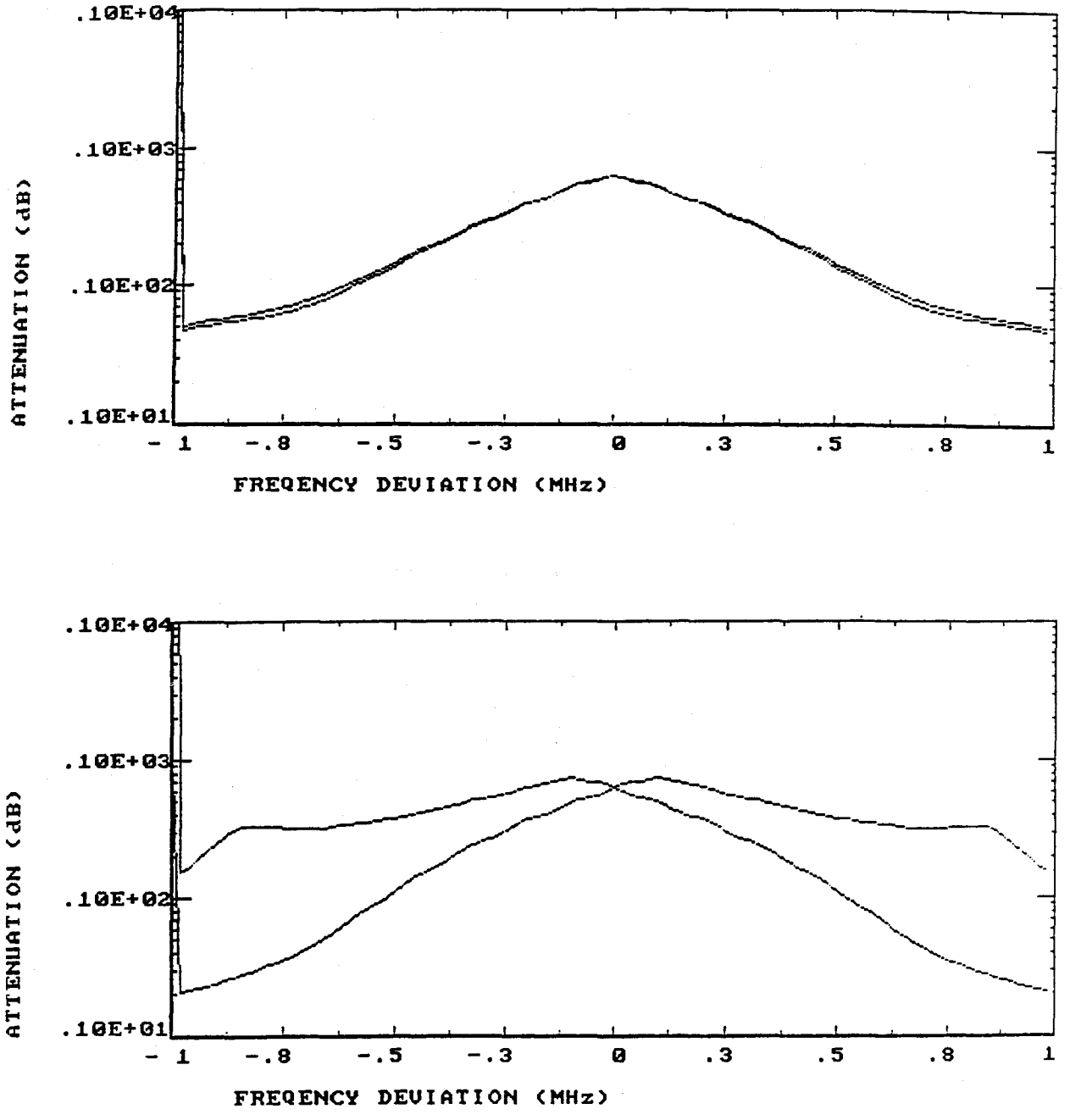


Figure 21. Total attenuation versus frequency deviation for waves emerging from the top of the mesosphere. Initial conditions are those of the Default Case. Top: vertical polarization beginning above and crossing beneath horizontal polarization. Bottom: right circular polarization beginning above and crossing beneath left circular polarization.

tions: vertical and horizontal, left and right circular. The horizontal polarization may be replaced by any elliptical polarization of interest.

## 5. CONCLUSIONS

At the pressures that exist in the mesosphere, the oxygen absorption lines near 60 GHz are still important but are so sharp that the geomagnetic field can effect a Zeeman splitting. Because of its nature this phenomenon converts the atmosphere into an anisotropic medium, thus making electromagnetic propagation more complicated than is usual.

We have seen how the medium can be modeled and how this model can be used to predict radio wave behavior. It turns out that a wave is likely to tend asymptotically to a wave with a particular polarization and while doing so, to exhibit a kind of Faraday rotation.

We have also described a computer program that will calculate many of the new entities that this anisotropy has made important. The program can be used to explore some of the novel features that have arisen and perhaps to help in the engineering design of radio systems that will use this medium.

## 6. ACKNOWLEDGMENT

The authors would like to acknowledge with gratitude the help provided by Andrew Katz. It was he who designed and wrote most of program ZEEMAN.

## 7. REFERENCES

Barraclough, D. R. (1985), International Geomagnetic Reference Field, revision 1985, Pure Appl. Geophy. 123, pp. 641-645.

Beckmann, P. (1968), The Depolarization of Electromagnetic Waves (Golem Press, Boulder, CO).

Born, M., and E. Wolf (1959), Principles of Optics (Pergammon Press, New York, NY).

COESA, U.S. Committee on Extension to the Standard Atmosphere (1976), U.S. Standard Atmosphere 1976, NOAA-S/T 76-1562, U.S. Gov. Printing Office, Washington, D.C., Sup. Docs. Stock No. 003-017-00323-0.

Courant, R., and D. Hilbert (1953), Methods of Mathematical Physics (Interscience Publishers, New York, NY).

Endo, Y., and M. Mizushima (1982), Microwave resonance lines of $^{16}O_2$ in its electronic ground state, Jap. J. Appl. Phys. 21, pp. L379-L380.

Gautier, D. (1967), Influence du champ magnétique terrestre sur le transfert du rayonnement millimétrique dans l'oxygène moléculaire de l'atmosphère, Geophysique 23, pp. 535-568.

Hartmann, G. K., and K. F. Künzi (1983), The Zeeman effect of $O_2$ and its influence on the brightness temperature of the Earth's atmosphere, MPI-Aeronomy Rpt. MPAE-W-66-22, Lindau, FRG.

Lenoir, W. B. (1968), Microwave spectrum of molecular oxygen in the mesosphere, J. Geophys. Res. 73, pp. 361-376.

Liebe, H. J., G. G. Gimmestad, and J. D. Hopponen (1977), Atmospheric oxygen microwave spectrum--experiment versus theory, IEEE Trans. Ant. Prop. AP-25, pp. 327-335.

Liebe, H. J. (1981), Modeling attenuation and phase of radio waves in air at frequencies below 1000 GHz, Radio Sci. 16, pp. 1183-1199.

Liebe, H. J. (1983), An atmospheric millimeter wave propagation model, NTIA Report. 83-137 (NTIS Order No. PB 84-143494).

Moler C., and C. VanLoan (1978), Nineteen dubious ways to compute the exponential of a matrix, SIAM Rev. 20, pp. 801-836.

Olivero, J. J., and R. L. Longbothum (1977), Empirical fits to the Voigt line width: a brief review, J. Quant. Spectrosc. Rad. Transf., 17 pp. 233-236.

Rosenkranz, P. W., and D. H. Staelin (1988), Polarized thermal microwave emission from oxygen in the mesosphere, Radio Sci. 23, pp. 721-729.

Townes, C. H., and A. L. Schawlow (1955), Microwave Spectroscopy (McGraw-Hill Book Co., New York, NY).

FORM **NTIA-29**
(4-80)

U.S. DEPARTMENT OF COMMERCE
NAT'L. TELECOMMUNICATIONS AND INFORMATION ADMINISTRATION

## BIBLIOGRAPHIC DATA SHEET

| | 1. PUBLICATION NO. | 2. Gov't Accession No. | 3. Recipient's Accession No. |
|---|---|---|---|
| | NTIA Report 89-249 | | |

4. TITLE AND SUBTITLE
MILLIMETER-WAVE PROPAGATION IN THE MESOSPHERE

5. Publication Date
September 1989

6. Performing Organization Code
NTIA/ITS.S1

7. AUTHOR(S)
George A. Hufford, Hans J. Liebe

9. Project/Task/Work Unit No.

8. PERFORMING ORGANIZATION NAME AND ADDRESS
National Telecommunications & Information Administration
Institute for Telecommunication Sciences
325 Broadway
Boulder, CO 80303

10. Contract/Grant No.

11. Sponsoring Organization Name and Address
Department of Defense
Code R 522
Ft. George Meade, MD 20755-6000

12. Type of Report and Period Covered

13.

14. SUPPLEMENTARY NOTES

15. ABSTRACT *(A 200-word or less factual summary of most significant information. If document includes a significant bibliography or literature survey, mention it here.)*

At heights between 30 and 100 km above the Earth, the oxygen absorption lines near 60 GHz together with the geomagnetic field cause the atmosphere to become an anisotropic medium. This report discusses why this is so and how to compute the consequent effects. It describes the computer program ZEEMAN, which allows the user to display in either graphical or tabular form many aspects of how radio waves propagate through this medium.

16. Key Words *(Alphabetical order, separated by semicolons)*
anisotropic media; millimeter waves; oxygen absorption lines; polaraization; radio propagation; Zeeman effect

| 17. AVAILABILITY STATEMENT | 18. Security Class. *(This report)* | 20. Number of pages |
|---|---|---|
| ☒ UNLIMITED. | | 62 |
| ☐ FOR OFFICIAL DISTRIBUTION. | 19. Security Class. *(This page)* | 21. Price: |

☆ U.S. GOVERNMENT PRINTING OFFICE: 1989—773-002/11,005 REGION NO. 8